AN EXPERIMENTAL STUDY ON THE BEHAVIOR OF SEGMENTAL PILES SUBJECTED TO LARGE LATERAL DISPLACEMENT

by

Ahmet Keklik

B.S., Civil Engineering, Istanbul Aydin University, 2016

Submitted to the Institute for Graduate Studies in
Science and Engineering in partial fulfillment of
the requirements for the degree of
Master of Science

Graduate Program in Civil Engineering

Boğaziçi University

2020

ACKNOWLEDGEMENTS

I would like to express my sincere gratitude to Prof. Gökhan Baykal, who is my thesis supervisor, for his guidance, support and encouragement throughout my thesis study.

I would like to thank Prof. Ayşe Edinçliler and Assoc. Prof. Kubilay Keleşoğlu for their valuable advices and supportive attitudes. I would also like to thank to research assistants and laboratory technicians for their help and kind attitudes.

The financial support provided by Boğaziçi University Scientific Research Fund (Project No: BAP 18A04P2) is acknowledged.The tests are conducted at the Boğaziçi University Karl Terzaghi soil laboratory with the help of research assistant Uğurcan Erginağ. The author would also like to thank Mr. Erginağ for his kind friendship and support.

I owe heartfelt gratitude to Barış Elmas for his continuously provided support and friendship throughout my master study. Also, the completion of the study would be very hard without the support of my dear friends, Serkan Apaydın, Ferhat Korul, and İbrahim Erkol especially in my difficult times.

Finally, I would like to thank to my dear father and sister for their encouragement and standing by me in whole of my life.

ABSTRACT

AN EXPERIMENTAL STUDY ON THE BEHAVIOR OF SEGMENTAL PILES SUBJECTED TO LARGE LATERAL DISPLACEMENT

Segmental model piles are composed of alternating concrete blocks and rubber sheets connected by a steel wire which can be tensioned to a desired force. One of the claims for these types of piles is the ability to undergo large horizontal displacements. To test this claim model segmental piles with 750N and 2250N tension force were placed into loose and medium dense sand and 50 mm lateral displacement was applied. The pile head load was measured. Magnetometers placed on each concrete block were calibrated to obtain the inclination of each block and an algorithm was developed to calculate lateral displacements along the pile from inclinations. The standard deviation of inclination values was 0.36, 0.60, and 1.71 degrees for 7.5, 15, and 22.5 degrees of inclination values respectively. Although the piles were classified as short piles, The 750N segmental pile demonstrated a flexible pile behavior for loose and dense sand conditions. The 2250 N segmental pile behaved similarly to that of a rigid pile for the loose sand condition. For the medium dense sand, the behavior changed to that of flexible pile. The horizontal capacity of 750 N pile reached to 500N for medium dense sand at 50 mm displacement coming close to 700N load measured for 2250N segmental pile under similar conditions. Both segmental piles did not show any structural failure signs under large lateral displacement.

ÖZET

EKLEMLİ KAZIKLARIN BÜYÜK YATAY DEPLASMANLARDAKİ DAVRANIŞI ÜZERİNE DENEYSEL BİR ÇALIŞMA

Eklemli model kazıklar, birbirini izleyen beton bloklar ve kauçukların istenilen kuvvetle gerdirilebilen çelik tel ile birbirine bağlanmasından oluşur. Bu kazıkların önemli avantajlarından biri, büyük yatay deplasmanlara kırılmadan dayanabilmesidir. Bu çalışmada, 750 N ve 2250 N ardçekme kuvvetine sahip eklemli kazık modellerin gevşek ve orta sıkılıktaki kumda yatay yükleme yapılarak 50 mm yatay deplasmana kadarki davranışları incelenmiştir. Kazık başı yükü ve kazığı oluşturan beton bloklarının üzerine yerleştirilen manyetometreler yardımı ile blok eğimleri ölçülmüş ve bu değerlerden kazığın yatay hareketi bir algoritma oluşturularak hesaplanmıştır. Eğimlerin standart sapması 7.5, 15 ve 22.5 derece için sırasıyla 0.36, 0.60 ve 1.71 olarak hesaplanmıştır. Kazıklar kısa kazıklar olarak sınıflandırılsa da, 750N segmental kazık gevşek ve orta sıkı kumda esnek bir kazık davranışı göstermiştir. 2250 N ardgermeli eklemli kazık, gevşek kum durumu için rijit bir kazığa benzer şekilde davrandığı gözlemlenmiş, orta sıkılıktaki kumda ise esnek bir kazık davranışı göstermiştir. Orta sıkılıktaki kumda 50 mm yatay deplasmanda 2250 N yüklü kazığın dayanımı 700 N, 750 N yüklü kazığın ise 500 N'a ulaşmıştır. Deneylerde kullanılan iki kazıkta da yüksek deplasman değerlerine rağmen herhangi hasar meydana gelmemiştir.

TABLE OF CONTENTS

LIST OF FIGURES

LIST OF TABLES

LIST OF SYMBOLS

c	Undrained shear strength
C_c	Coefficient of curvature
C_u	Coefficient of uniformity
C_x	Calibrated magnetometer value in x direction
C_y	Calibrated magnetometer value in y direction
C_z	Calibrated magnetometer value in z direction
cm	Centimeters
D	Diameter
D_r	Relative density
E	Young modulus
E_s	Soil subgrade modulus
E_p	Modulus of elasticity of pile
EI	Flexural rigidity
F	Force
GNm^2	GigaNewton square meter
I	Moment of inertia
k	Soil modulus
K_p	Passive lateral earth pressure coefficient
kPa	Kilopascal
L	Length
m	Meters
min	Minute
mm	Milimeters
N	Newton
p	Soil reaction
P	Applied load
R_u	Bending moment versus depth
s	Sensor

s	Slope
V	Shear Force
y	Horizontal displacement at a significant depth
z	Depth
ν	Poisson ratio
ϕ	Internal friction angle

LIST OF ACRONYMS/ABBREVIATIONS

ASTM	American Society for Testing and Materials
BNWF	Beam on Nonlinear Winkler Foundation
DISPL	Displacement
IDE	Integrated Development Environment
K_{rc}	Relative Stiffness Factor
LVDT	Linear Variable Differential Transducer
MAX	Maximum
NA	Not Applicable
PCB	Printed Circuit Board
SP	Poorly Graded Sand
SD	Standard Deviation
SPVFR	Segmental Piles with Variable Flexural Rigidity
TAM	Three-axis Magnetometer

1. INTRODUCTION

Pile foundations are one of the most common and oldest foundation types in geotechnical engineering. In cases where the shallow foundation is insufficient to carry loads of superstructure, pile foundation is an alternative to transfer the loads to deep layers safely. Although pile foundations are generally designed to transfer vertical loads, lateral loads may be a problem as well. Wind, seismic loading, land sliding, and impact loading are common lateral loads. Common laterally loaded pile foundation applications are shown in Figure 1.1. Pile behavior under vertical and lateral loading is quite different because of the non-linear behavior of laterally loaded piles. Hence, the measurement of horizontal displacement with depth is important to understand the behavior. Comparison of vertical and lateral loading is shown in Figure 1.2 [3] [17] [1].

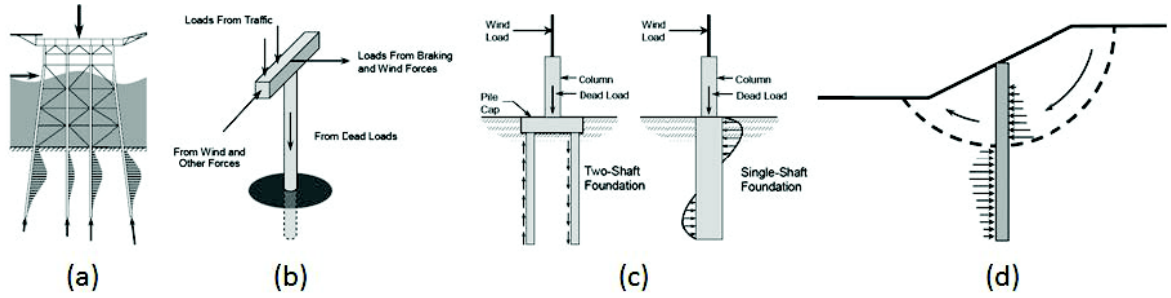

Figure 1.1. Laterally loaded pile foundation applications: (a) Offshore applications, (b) Single pile support for a bridge, (c) Pile supported overhead sign, (d) Piles to stabilize slopes [1].

Flexural rigidity of the pile is and one of the most important parameters in the design of laterally loaded pile. Studies regarding flexural rigidity were published by many researchers [10] [5] [19]. However, flexural rigidity was evaluated with other parameters (pile geometry, configuration, and spacing of pile group, soil properties, the roughness of pile, overburden pressure, etc.) in these researches and the range of flexural rigidity values of testing piles was not so comprehensive since the high rigidity of the test materials such as steel, aluminum, and concrete was used as pile material.

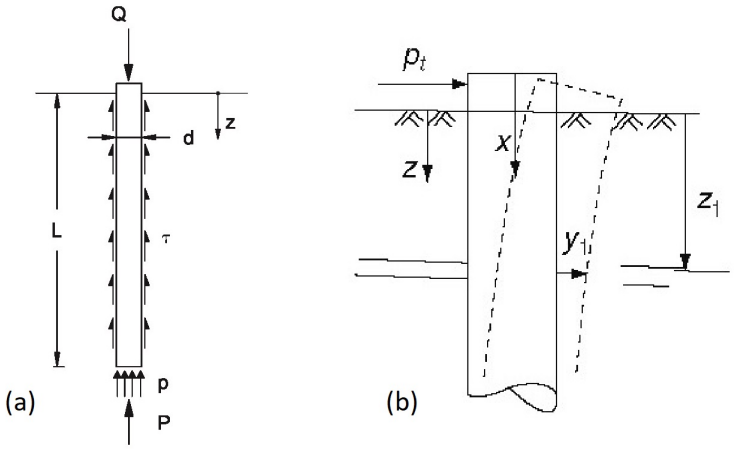

Figure 1.2. (a) Vertical loading [2] and (b) lateral loading of pile [3]

.

In this thesis study, in order to understand the effect of flexural rigidity of laterally loaded piles, a series of experiments were conducted under laboratory conditions. In this context, model piles with varying flexural rigidities were produced. To produce these model piles, segmental elements were used. These produced piles are named as "Segmental Piles With Variable Flexural Rigidity (SPVFR)" [20] [11]. SPVFR allows to adjust flexural rigidity and can undergo large lateral displacements without breakage. In order to attempt to monitor the horizontal displacement of the pile, inclinations of each segment of the pile were measured by using the magnetometers and Arduino board economically. Additionally, a code was developed with a programming language (Python) to process data obtained from the experiments. Obtained data were evaluated and compared with the studies in the literature.

2. LITERATURE REVIEW

In this chapter, the literature review summarizes the researches on the behavior of laterally loaded piles and laboratory tests about laterally loaded piles.

2.1. Analysis of Laterally Loaded Piles

Various methods were developed to analyze laterally loaded piles. These methods have ranged from basic empirical equations and tables to three-dimensional soil models. Although with basic methods, results can be obtained quickly, the accuracy of analysis can not be sufficient. Various methods will be reviewed in this section.

2.1.1. Simplified Methods

Brinch Hansen [21] published a method to calculate the ultimate lateral capacity of piles. In this method, based on earth pressure theory, cohesion and internal friction angle are used to calculate soil resistance to lateral loads. The method assumed that there is no yield hinge and pile rotates as a rigid body. Therefore, the method is applicable only to short piles.

Another simplified method that is based on charts, graphs and simple equations was proposed by Broms [4] [22] [23]. With this method, lateral load capacity of a single pile can be calculated for cohesive and granular soils, but the disadvantage of this method is that pile in layered soil cannot be calculated. The method can be used for rigid or flexible and free-head or fixed-head piles.

2.1.2. Subgrade Reaction Method

Subgrade reaction method based on Winkler's assumptions [24] suggests that an increase of the displacement of the pile horizontal displacement (y) causes linear increment on soil reaction (p) and the subgrade modulus E_s is defined as -p/y. Hetenyi [25]

proposed one of the first simple approaches for laterally loaded pile behavior based on subgrade modulus. Hetenyi assumed that E_s is constant with depth like Granholm [26]. Also, Terzaghi [27] presented a formulation to determine subgrade modulus for over-consolidated clays, and this value is assumed constant with depth for overconsolidated clays.

Matlock and Reese also presented effective solutions for laterally loaded piles from 1955 to 1970. One of the first comprehensive attempt to understand laterally loaded piles was proposed by them for both rigid and flexible piles [28]. The study determines pile displacement, pile rotations, bending moments, shear forces, and soil reactions and the method assumes that E_s changes nonlinearly. In order to determine these values, a differential equation was developed. Also, Palmer and Thompson [29], and Davisson and Prakash [30] proposed E_s varies nonlinearly.

2.1.3. P-y Curve Method

With the significant increase in offshore platform installation in the late 1950s, studies about laterally loaded piles increased. A significant amount of full scale laterally loaded pile tests sponsored by the petroleum industry was conducted. These tests and studies resulted in the development of p-y curve method. P-y curve method uses non-linear relationship between soil resistance (p) and lateral displacement (y) at specific depth as shown in Figure 2.1 [31]. The concept was introduced by McClelland and Focht [32] in 1956 and finite difference method was used to solve beam moment equations. They performed full-scale steel pipe pile tests and laboratory tests. As a result of the tests, a correlation method was suggested to predict p-y curve from triaxial laboratory tests.

Studies were conducted on saturated soft clay Matlock [33], saturated stiff clays Reese et al. [34], unsaturated clays Reese and Welch [35] to develop p-y curves. Also, Reese et al. [36] conducted full-scale tests under static and cyclic loading to develop p-y curves for laterally loaded piles in sand. Lee and Gilbert [37] conducted full-scale laterally loaded tests in very soft organic clay and peat. Octagonally shaped steel piles

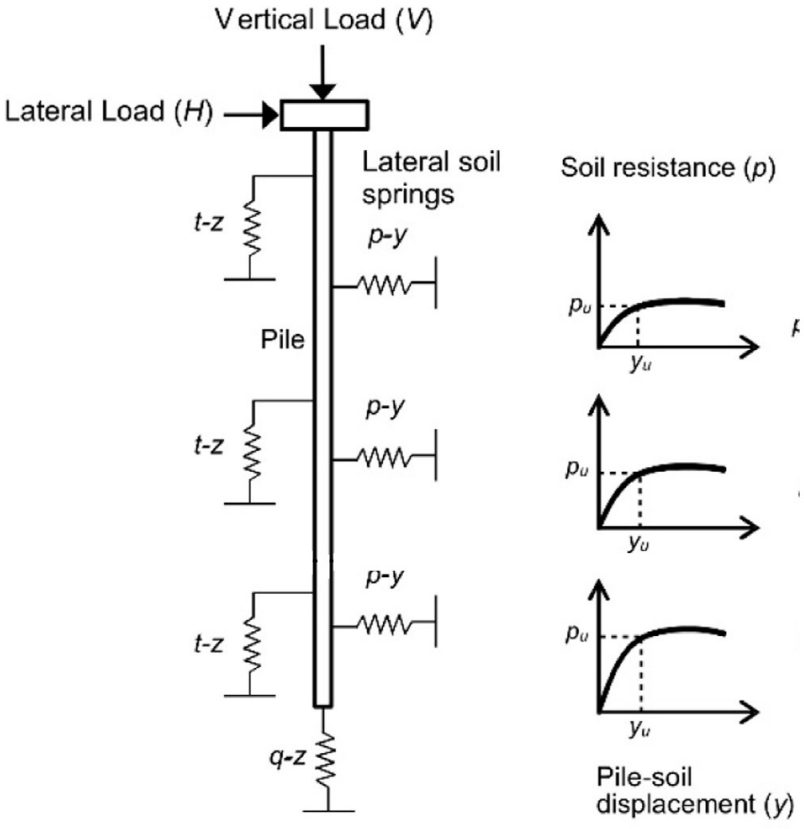

Figure 2.1. BNWF model of pile-soil interaction and p-y curves.

were loaded as short-term static, cyclic, unloading-reloading, and load to failure above 18 meters from ground line.

Georgiadis [38] conducted a study in order to develop p-y curves in layered soils. The method is based on equivalent depth calculation for each stratum as a function of actual depth, overburden pressure, and soil properties of soil layer. To calculate pile response to lateral load the COM64 software was used. Chong et al. [39] presented a study about the effects of joints in the determination of p-y behavior and the laterally loaded piles socketed into mudstone.

Zhang et al. [40] proposed a study to develop nonlinear p-y curves for single batter pile in sand. In this study, the effects of pile batter and soil density on lateral resistance were studied based on centrifuge test results. Also, Zhang et al. [41] presented a nonlinear continuum method to predict load-displacement response of drilled shafts under lateral loading in the soil layer whose deformation modulus varying linearly with depth overlying a rock mass.

Mokwa et al. [42] conducted a series of laterally loaded tests in partially saturated silts and clays and compared with the results of software that was LPile 3.0 (1997). Also, p-y curves were predicted based on Evans and Duncan's formulation [43] and compared with measured load-displacement curves. According to the study, the default p-y curve method predicts soil resistance less than the measured loads, and the required load to displace the pile is more than the measured loads.

Rollins et al. [44] presented p-y curves for laterally loaded piles in liquefiable soils. To investigate pile-soil-pile interaction, full-scale laterally loaded pile group blast-induced tests in liquefiable soils were investigated. Also, a single pile test was conducted for comparison and it was shown that each pile in the group had the same lateral resistance. Also, a study presented by Chang and Hutchinson [45] aimed to investigate p-y curve during pore pressure buildup. Single steel pile in homogeneous saturated sand was subjected to sequential dynamic shaking and lateral loading in order to obtain sufficient data to develop p-y curve for liquefaction soil conditions.

Zhu et al. [46] introduced an experimental and analytical model for laterally loaded rigid monopiles in low liquid limit silt. 6 tests were conducted in silts with 2 different relative densities to determine p-y curves. Tests displayed that the rotational center was between 0.75 and 0.85 of the embedded length of pile and work-hardening load-displacement curves. According to test results, new p-y curves were established using a coefficient of subgrade reaction that is correlated to the local pile displacement.

Scours are one of the most important problems for structures in water, which reduce the capacity of foundations. In practice scour effect on laterally loaded piles evaluated by ignoring the scour-hole dimensions. Lin et al. [47] developed a simplified method to analyze laterally loaded piles in soft clay under scouring conditions by modifying the p-y curves proposed by Matlock [33]. To test the simplified method, software relying on 3D finite difference method was used. Increase of the slope of scour increased the lateral pile resistance.

Suleiman et al. [48] conducted a study to investigate soil-pile interaction of laterally loaded piles under passive loading. To investigate the interaction between the pile and surrounding soil and load-displacement relationship, laboratory tests were conducted with precast concrete pile in well-graded sand with a sliding mechanism, stereo digital image correlation system to monitor three-dimensional movement, and tactile pressure sheets. The results of tests were compared with p-y curves developed according to Broms' [22] and Ito and Matsui's [49] method to predict p-y curve. According to the results of the study, Broms' method overestimates the ultimate lateral resistance, and Ito and Matsui's method underestimates ultimate lateral resistance. The behavior of a passive pile under lateral loading is shown in Figure 2.2.

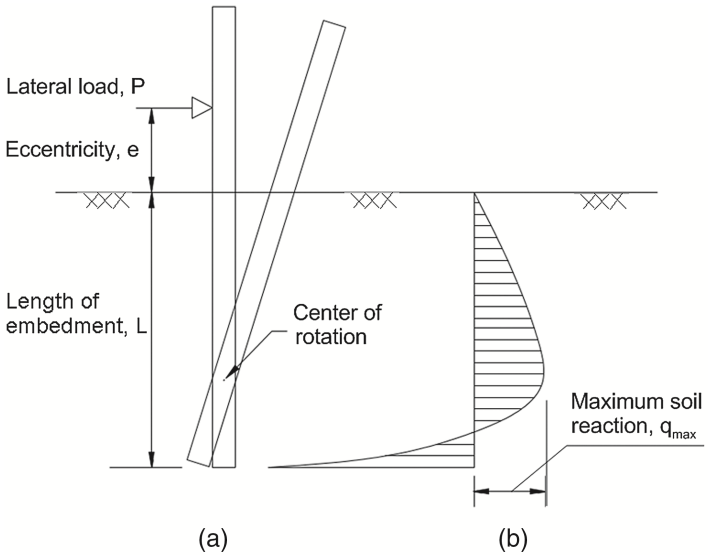

Figure 2.2. Failure mode of a short free-headed pile: (a) displacements; (b) distribution of soil reactions [4].

2.1.4. Elastic Continuum Method

Subgrade reaction method does not consider soil's continuity, therefore several solutions were proposed based on Mindlin's three-dimensional elasticity equations [50]. As for elastic continuum methods, the soil is modeled with linear and nonlinear springs that represent soil more realistic. Spillers and Stoll [51] proposed a simplified theoretical method for pile in linear, isotropic, and both elastic half-space and plastic half-space taking account of non-linearity.

Poulos [52] [53] [54] also presented a solution for floating and socketed laterally loaded piles in ideal homogeneous, isotropic, semi-infinite elastic soils and it is assumed that pile does not affect the soil properties. The pile is segmented to equal size parts except for first and final segments that are half-length of other segments. For each segment horizontal stress is uniformly distributed. Cross-section and elasticity modulus of pile are constant. The method was proposed for rectangular or I cross-sectional pile but circular cross-sectional piles approximation is possible.

Boundary element method is used and for each element horizontal displacements are calculated with Mindlin equations to calculate pile displacement. To calculate the effects of the pile to pile influence factor is used. The method can be used for only homogeneous soils because there is no Mindle equation for layered soils. Poulos [55] improved his continuum method.

Banerjee and Davies [56] used boundary element method to bistratum elastic half-space soil and soil modulus increases linearly with depth. The method was compared with full-scale tests and the results were more realistic because of the linear increment of soil modulus. Davies and Budhu [57], Budhu and Davies [58] [59] also adapted the method of Banerjee and Davies to the nonlinear behavior of laterally loaded piles for clay and cohesionless soils.

Randolph [60] has presented a parametric study that used finite element method and assuming that soil behaves as a continuum elastic and its elasticity modulus varying linearly. This linearity can be presented as a simple expression that considers the effect of neighboring piles. Randolph suggested characteristic shear modulus (G_c) that is the average value of shear modulus overactive length of the pile and critical depth (l_c) for flexible piles.

2.1.5. Simplified Continuum Models

Sun [61] proposed a numerical approach and parametric study to calculate soil and pile interaction under lateral load. Variational calculus was used to get differential equations of soil that assumed linear homogeneous elastic and pile system. Sun basically has adopted Vallabhan and Das's work [62]. The method considering both fixity of head and tip uses a principal parameter (γ) an iterative technique was adopted to obtain minimum of potential energy. To calculate the lateral reaction of the pile, lateral non-dimensional displacement was used. Zhang et al. [41] developed a non-linear continuum method to calculate stress behavior of laterally loaded drilled shafts. Their approach adopts and extends Sun's method [61]. While in Sun's model, soil behavior is homogeneous elastic, Zhang et al. [41] have considered yielding.

Guo and Lee [63] also presented a two-parameter model to predict lateral load-displacement relationship at laterally loaded piles like Sun. A disadvantage of the former two-parameter models is that when Poisson's ratio is high, obtained results may be unreliable. To overcome this disadvantage, they introduced a rational stress field. Variation of Poisson's ratio was included with characteristic shear modulus (G_c) proposed by Randolph [60]. Basu and Salgado [64] also proposed a study to analyze laterally loaded piles in multilayered soil based on Sun's model.

2.1.6. Displacement-dependent Lateral Earth Pressure

Mei et al. [16] proposed a model to predict displacement-dependent lateral earth pressure. Retaining structure movement and earth pressure can be predicted with the model for any condition intermediate to the active and passive states. The curve-fitting model is shown in Equation (2.1) should be satisfied with four conditions that are:

(i) The earth pressure is equal to the earth pressure at-rest at a displacement of s = 0,
(ii) The model is a monotonically increasing function of the displacement s,
(iii) The model is a bounded function for $s_a \leq s \leq s_p$,
(iv) The point s = 0 is an inflection point at which the curve changes from being concave upwards to concave downwards

$$p_s = [\frac{k(\phi)}{1 + e^{-b(s_a,\phi)}} - \frac{k(\phi) - 4}{2}]\frac{p_0}{2} \tag{2.1}$$

where ϕ is the soil friction angle, k(ϕ) is a function of soil friction angle, p_s is the lateral earth pressure,p_0 is the lateral earth pressure at-rest ,b(s_a,ϕ) is a function displacement required to mobilize the minimum active earth pressure and friction angle.

2.2. Rigid and Flexible Piles

Flexural rigidity is one of the major parameters to determine pile behavior under horizontal loading. Matlock and Reese [28] have proved that the rigidity of a pile is dependent on the ratio of the flexural stiffness of the pile, and the foundation soil modulus. To classify pile behavior, the pile-flexibility factor (K_{rc}) was defined as the flexibility of the pile relative to the soil by Poulos et al. [17]. K_{rc} has limiting values of infinite for an infinitely rigid pile and zero for an infinitely long pile. Equation of K_{rc} is shown in Equation 2.2 and classification is shown in Table 2.1.

$$K_{rc} = \frac{E_p I_p}{E_s L^4} \tag{2.2}$$

Table 2.1. Values for K_{rc} [17].

Classification	**K_{rc}**
Very flexible	$<10^{-5}$
Relatively flexible	$<10^{-3}$
Relatively stiff	$>10^{-2}$
Stiff	$>10^{-1}$

2.3. Laboratory Tests

Researches including laboratory experiments on laterally loaded piles are listed in Table 2.2. The pile materials used in experiments are steel, aluminum, and concrete and the soils are clay and sand at various relative densities. Single and group pile experiments were conducted to understand the behavior of laterally loaded piles.

Table 2.2. Summary of laboratory model tests [18].

Dimensions of Tank (m)	**Soil**	**Pile material**	**Pile diameter (mm)**	**L/D**	**Pile Installation**	**Max. Displ. (mm)**	**Reference**
NA	Clay	Steel and aluminum	12.7-25.4	20-40	Preinstalled	10	Rao et al. [5]
NA	Sand	Aluminum	12.7	NA	NA	NA	Prakash [65]
0.45x0.45x0.35	Sand	Steel	12.5	16	Preinstalled	33	Meyerhof et al. [66]
0.9x0.75x0.9	Sand	Aluminum	20	12 & 38	Preinstalled	20	Patra and Pise [8]
0.8x0.8x0.6	Sand	Steel	12	20	Preinstalled	8	Kim and Yoon [10]
1.8 (D) - 2 (H)	Sand	Steel	102	11	Preinstalled	100	Prasad et al. [9]
0.9x0.7x0.65	Sand	Aluminum	15.88	32	Preinstalled	17	Khari et al. [7]
1.8x1.8x1.8	Sand	Steel	102	15	Preinstalled	60	Hai Lin et al. [67]
NA	Sand	Steel and aluminum	16	18	Preinstalled	NA	Chawhan et al. [68]
NA	Clay	Steel and concreate	50-100	10-20	Preinstalled and Bored	20	Mohamedzein et al. [69]
1 (D)	Clay	Steel and concrete	51,89,175	5-8	Bored	37	Mayne et al. [6]

Rao et al. [5] proposed a study to investigate the effects of the pile rigidity, embedment length, and pile arrangement on laterally loaded pile groups in marine clay with an experimental program. For tests, pile groups were modeled at laboratory, aluminum and mild steel were used as the material of piles. A test tank filled with marine clay was used to simulate soil conditions. Aluminum and steel materials have 0.754 x 10^8 and 2.1 x 10^8 kPa modulus of elasticity (E) and 0.30 poisson's ratio, respectively. The results showed that the behavior of laterally loaded pile groups depends on essentially critical space which is a function of embedment depth of piles and the arrangement of piles concerning the direction of loading. Moreover, it was shown that the optimum arrangement of the pile is dependent on the flexibility of piles; rigid piles are more resistant to lateral loads when arranged parallel and long flexible piles are more resistant when arranged in series. Load-displacement curves of the single aluminum piles are shown in Figure 2.3. The maximum lateral displacements of the pile head were 0.3 pile diameters. Also, the experimental setup of Rao et al. is shown in Figure 2.4.

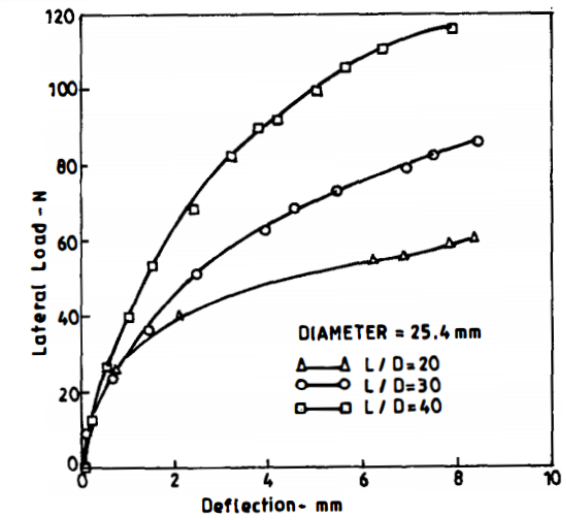

Figure 2.3. Load-displacement curves of the single aluminum piles [5].

Mayne et al. [6] conducted a series of laboratory tests in order to investigate the effects of shaft diameter, shaft material, shaft geometry, and load eccentricity on the behavior of free-head drilled shafts under lateral loading. 28 Cast-in-place concrete shafts with 51, 89, and 175 mm diameters were constructed and tested in consolidated

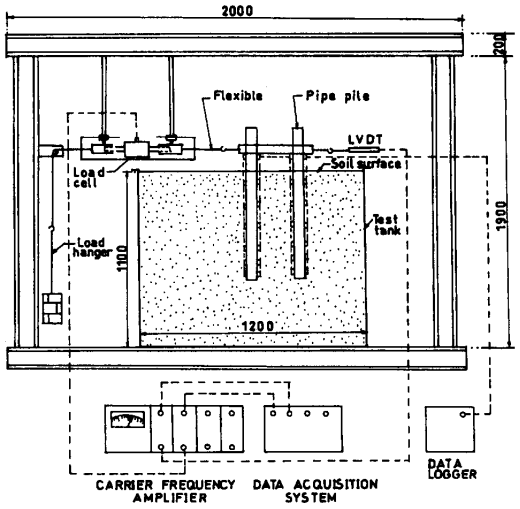

Figure 2.4. Experimental setup of Rao et al. [5].

clay under nonlinear, monotonic, and static lateral loads. As a result, it was observed that the behavior of laterally loaded shafts is highly nonlinear but can be represented as a hyperbola, ultimate lateral capacity increases with depth, and diameter decreases with the eccentricity of load. Also, shaft surface roughness increases the capacity and stiffness of the shaft under lateral loading.

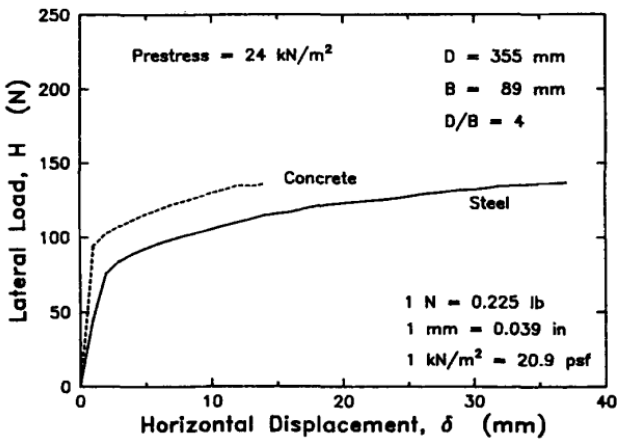

Figure 2.5. Effect of shaft material on lateral load-displacement response [6].

Khari et al. [7] proposed a study to investigate the effects of spacing, relative density, and arrangement of piles on ultimate lateral resistance and group efficiency of laterally loaded pile groups in sand. Experimental investigations were conducted with laboratory model pile tests in rectangular test tank had 700mm width, 900mm length, and 650mm height dimensions. Piles were produced open-end and hollow circular aluminum alloy. To measure displacements Linear Variable Differential Transducers (LVDT) were used. It was observed that when s/d increased from 3 to 6 ultimate lateral load increased 53%. When the number of piles increases group efficiency decreases because of overlapping of zones and active wedges and 6 times of diameter spacing is enough to eliminate pile-to-pile interaction. Like Rao et al. [5], they reached flexible piles of series arrangements that provide more resistance than that obtained from the parallel arrangement. The load-displacement curves of the single pile are shown in Figure 2.6. Maximum lateral displacements of the pile head were 1.1 pile diameters for 30% and 70% relative densities.

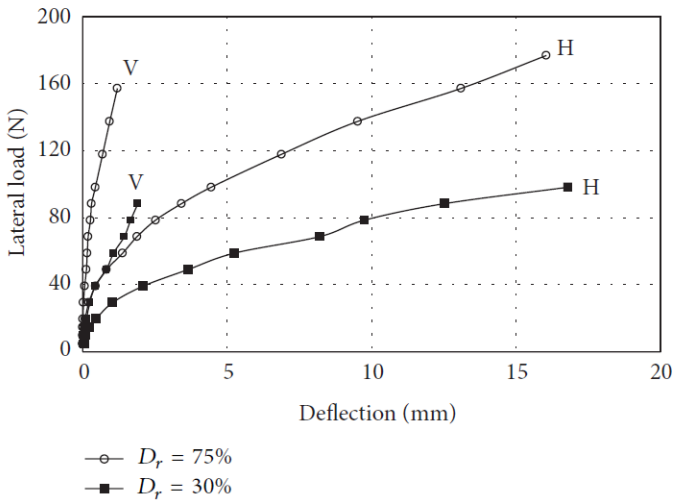

Figure 2.6. Lateral load versus displacement diagram for single pile (H = horizontal; V = vertical) [7].

Patra and Pise [8] presented series of static lateral load tests on prototype-scale piles in the sand to investigate the effect of pile friction, group geometry, spacing of piles in group, and relative density on the behavior of laterally loaded pile group. As

model pile aluminum alloy tubes and to simulate soil conditions a test tank that has 914 mm length, 762 mm width, and 914 mm depth were used. As a result, the ultimate lateral capacity of the pile group depends on the length-to-diameter ratio of pile, pile friction angle, pile group geometry, spacing of piles in a group and, sand placement density. Like Khari et al. [7], that six times of pile diameter is enough to eliminate the pile group effect was a result of the study. Lateral load versus lateral displacement diagram is shown in Figure 2.7. The maximum lateral displacement values of the pile head were 0.5 to 1 pile diameters.

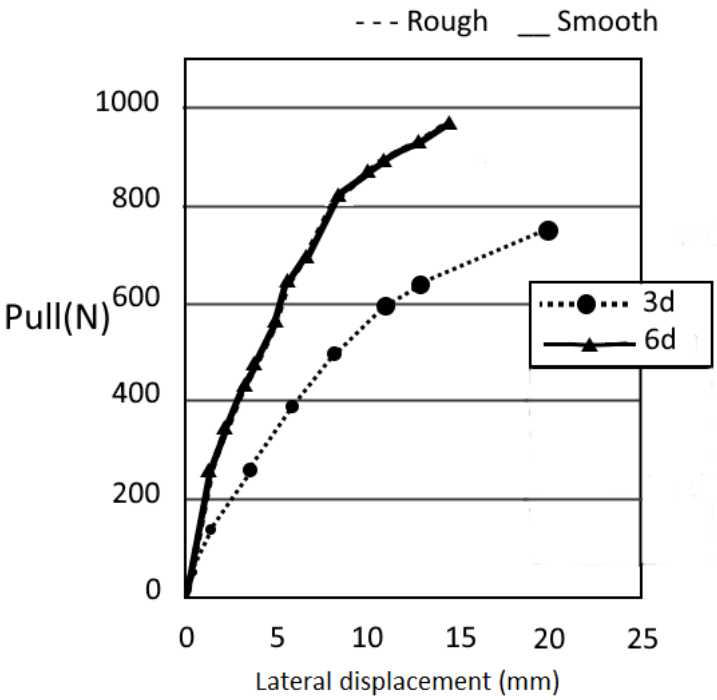

Figure 2.7. Lateral load versus lateral displacement diagram for pile group [8].

Prasad et al. suggest a method to predict soil pressure distribution and ultimate lateral resistance of rigid piles in granular soils. Also, in order to validate the method experiments were conducted with a smooth steel model pile in well-graded angular sand. The model pile has 102 mm diameter, 1135 mm length and 2.1 x 10^8 kPa modulus of elasticity. Test results are shown in Figure 2.8.

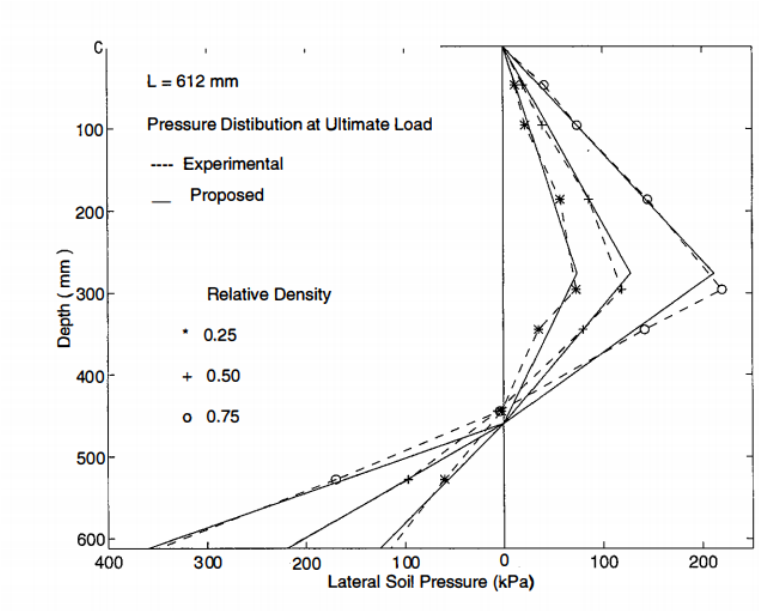

Figure 2.8. Soil pressure distribution at ultimate load of Pradas et al. [9].

Kim and Yoon [10] performed laboratory model pile tests to investigate pile group interaction effects in the sand. Six types of pile configurations and 3 to 8-diameter pile spacing were used to understand the effect of pile group configuration on pile behavior.The model pile has 2.1 x 10^{10} kPa modulus of elasticity and 45 GNm^2 flexural rigidity (EI). The test tank has 80 cm length, 80 cm in width, and 60 cm in depth. Experimental set-up is shown in Figure 2.9. The experiment results are shown in Figure 2.10. According to the results, the relative density of soil increase pile resistance directly both single pile and pile groups.

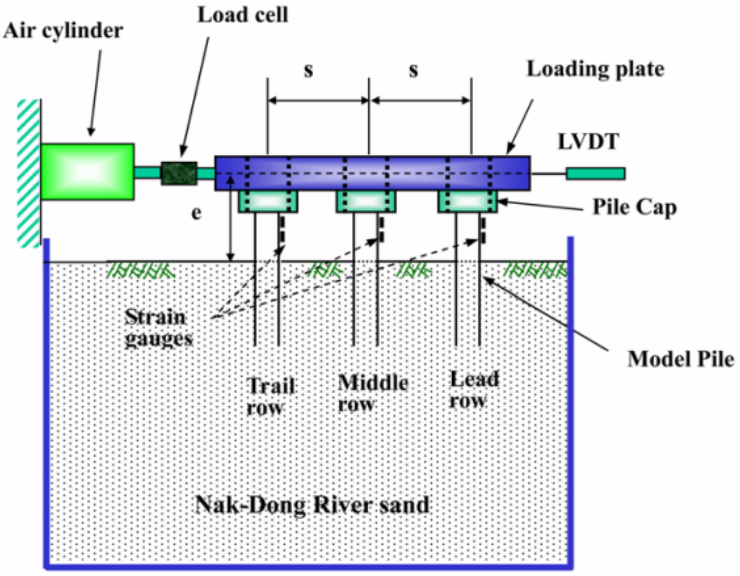

Figure 2.9. Side view of layout for static fixed-head test [10].

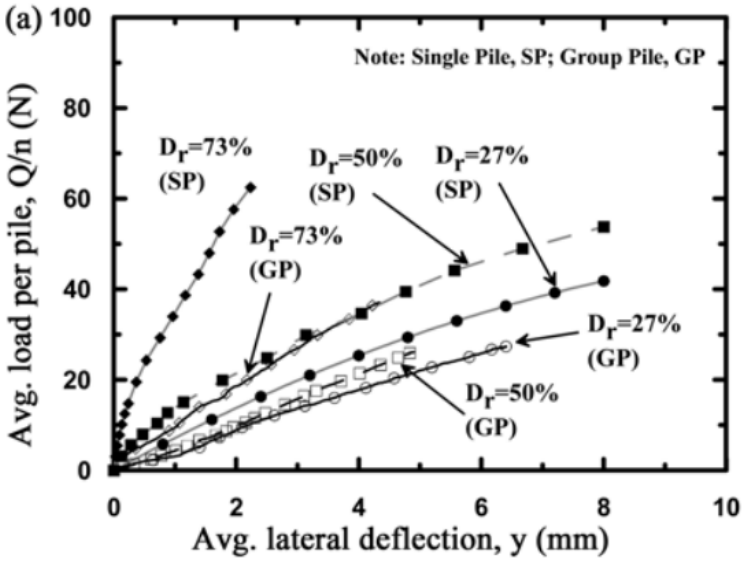

Figure 2.10. Average lateral load-displacement response for group tests with varying relative density and single pile tests for 3d pile spacing [10].

Research shows that the relative density of soil affects pile behavior directly. In loose to medium sand lateral displacement of the pile is larger than that of medium

to dense sand under the same lateral load. The load distribution ratio versus lateral displacement in medium dense sand is shown in Figure 2.11. The maximum lateral displacement of the single pile head was approximately 2mm to 7 mm.

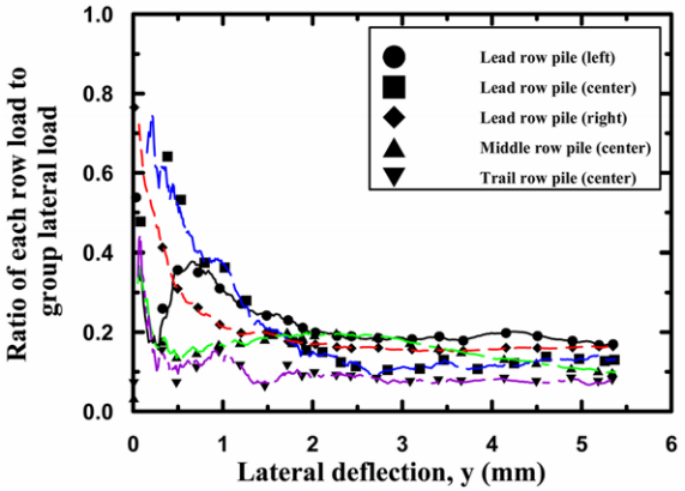

Figure 2.11. Variations of load distribution ratio with lateral displacement in medium dense sand [10].

2.4. Previous Researches About SPVFR

SPVFR, a segmental pile with variable flexural rigidity, is a pile model composed of mortar blocks and rubber pads with a cable passing through the center of components to provide post-tension to the pile. Baykal [20] has developed the Segmental Pile concept at Boğazici University and tests were conducted to determine the applicability of the concept by Yahia [11]. Flexural rigidity of the pile can be adjusted with changing post-tension. SPVFR is shown in Figure 2.12 .

Figure 2.12. Segmental pile with variable flexural rigidity [11].

Baykal et al. [20] [11] proposed a study to create and investigate the behavior of SPVFR under lateral loading. To construct SPVFR, a steel wire passed holes of mortar blocks and rubber packs, and two aluminum profiles were placed at the two ends of the SPVFR as a bearing plate. To provide flexural rigidity to the pile, steel wire was post-tensioned with three loads that are 750, 1500, and 2250 N.

A series of laboratory tests were conducted to investigate the flexural rigidity of SPVFR, stress distribution on mortar block surfaces, and behavior of SPVFR under lateral loading under laboratory conditions. The modulus of elasticity in bending E_f was obtained from three-point bending tests. Stress distribution on mortar blocks was measured by placing pre-scale films between mortar blocks.

Experiments to investigate the behavior of model pile under lateral loading were conducted on the Winkler foundation. The pile was fixed at one end and placed on springs to model soil. To form the foundation open-coil helical springs that have 4 N/mm stiffness were used. The model piles were loaded statically and cyclically at the top and the mid-point of piles. Displacement, spring reaction, boundary condition, shear force, and bending moment results along SPVFR for 1K, 2K, and 3K (K = 4 N/mm) static tests of 2250 N post-tensioned SPVFR are shown in Figure 2.13.

Sengez [12] also conducted a study on the lateral capacity of segmental SPVFR model piles under cyclic loading. By using the antagonistic testing device operate with pneumatic muscles, the model piles were loaded cyclically. 750, 1500, and 2250 N post-tensioned SPVFR model piles were tested in dry coarse sand by using a Large Displacement Constant Contact Area Shear Device [70]. The cap of single piles was loaded 300 N with 30-50-100 cycles and displacement with depth was measured with LVDTs. Five LVDTs were placed with 8.5 cm range and the test results in loose, medium, and dense sand are shown in Figure 2.14. The test results given by Sengez have flaws. The verification of results was not complete. The displacement measurements with transducers were not verified. The monolithic concrete pile shows similar displacement to that of the segmental pile which does not seem to be correct at have at low head load. The head loads were not measured by a load cell. No difference for loose to dense sand in observed in Figure 2.16 which is not likely.

Load-displacement curves top-head of the piles with 750 N and 2250 N post-tension in loose and medium-dense soil are shown in Figure 2.15. Also, as a reference, a mortar beam having the same dimensions with segmental piles was tested in the same soil and test result are shown in Figure 2.16. According to the test results of Sengez [12], the increasing relative density of soil causes a small decrease in the displacements and the increasing rigidity of the segmental pile causes a decrease in displacement. Also, load-displacement curves of mortar beam and segmental pile with 2250 N post-tension were close.

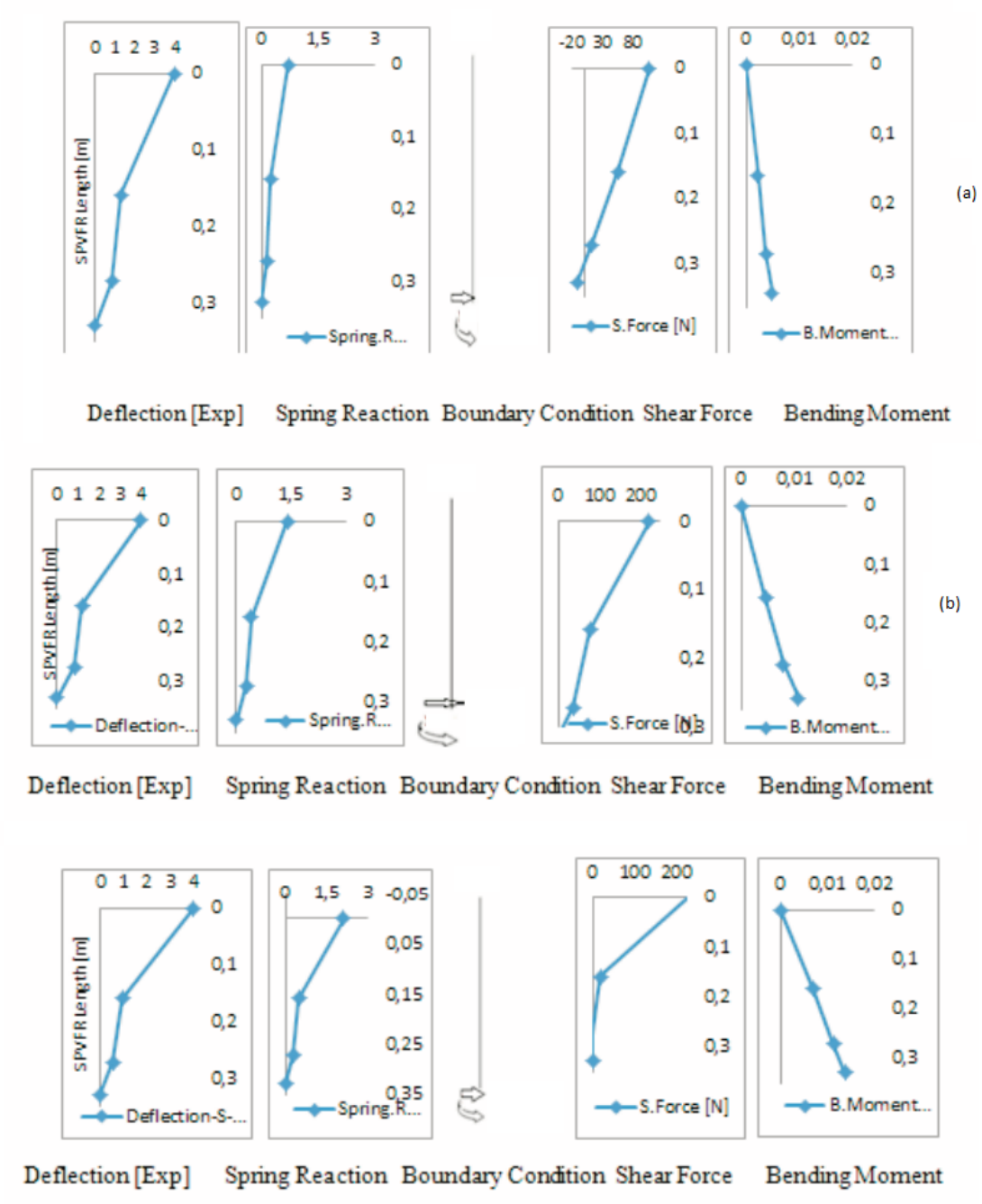

Figure 2.13. Displacement, spring reaction, boundary condition, shear force and bending moment along SPVFR placed on 1K (a), 2K (b) and 3K (c) for 2250 N pile [11].

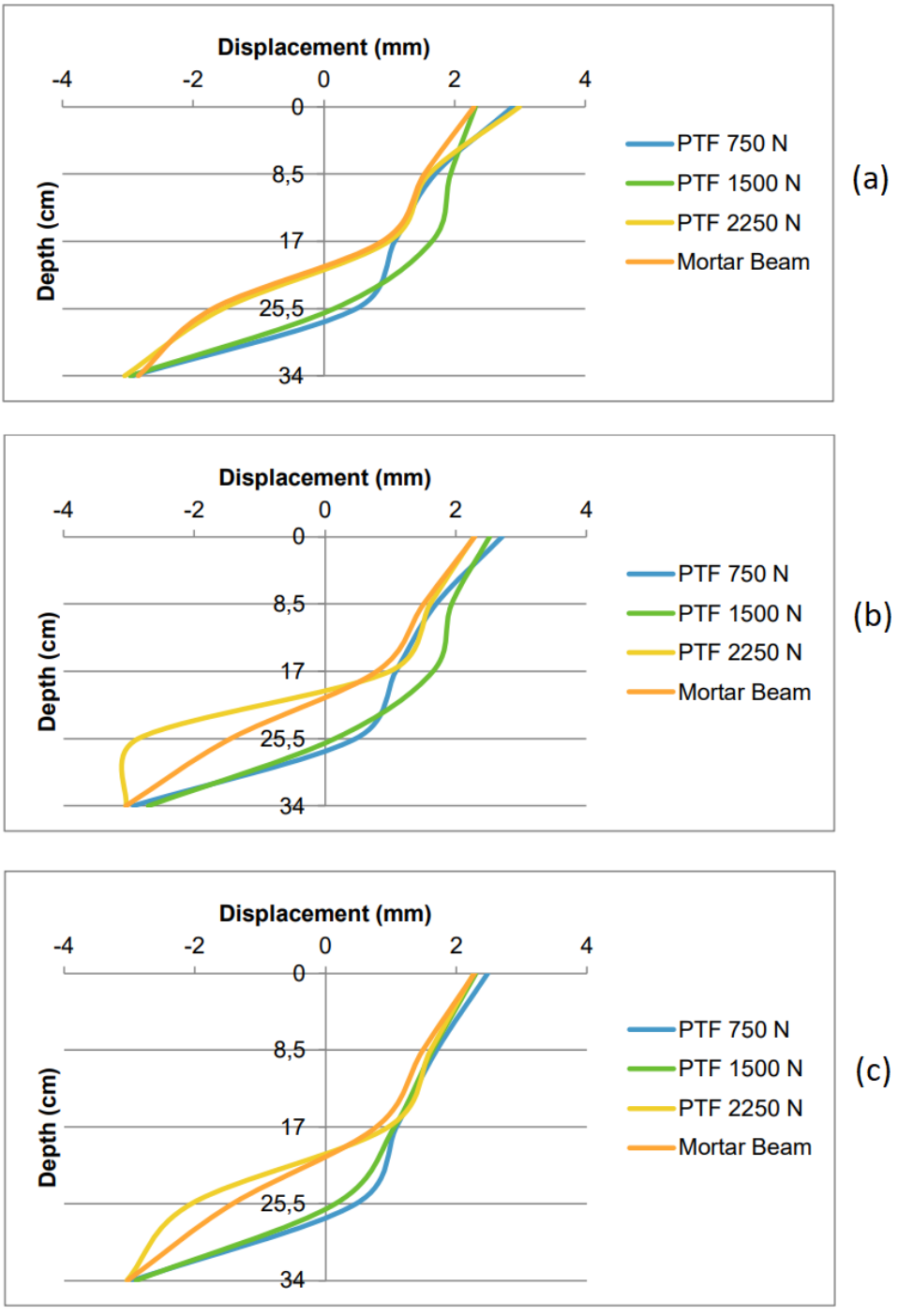

Figure 2.14. Displacement values of the piles in (a) loose (b) medium, and (c) dense soil [12].

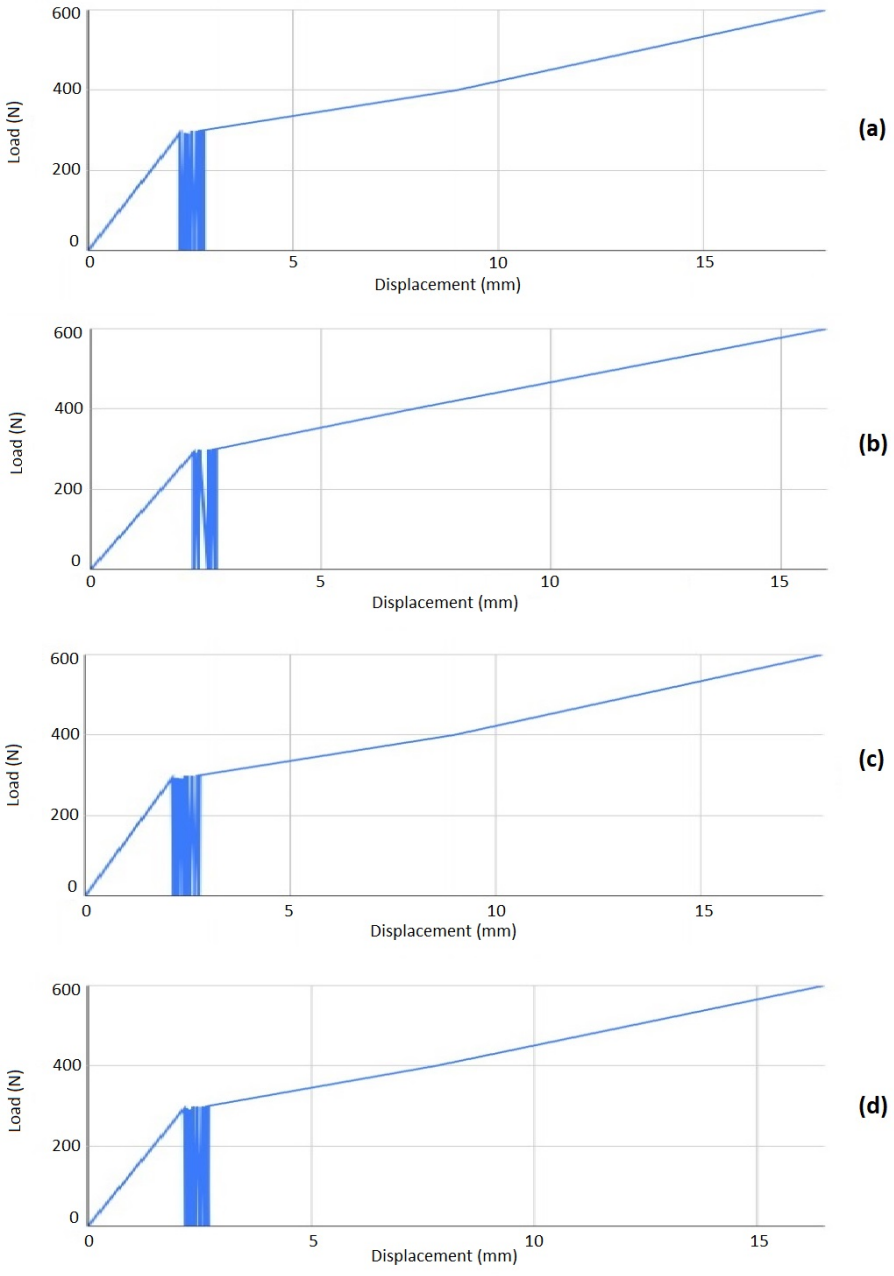

Figure 2.15. Load-displacement curves of top-point of the piles with 750 N post-tension in loose (a) and medium-dense (b) soils and 2250 N post-tension in loose (c) and medium-dense (d) soils [12].

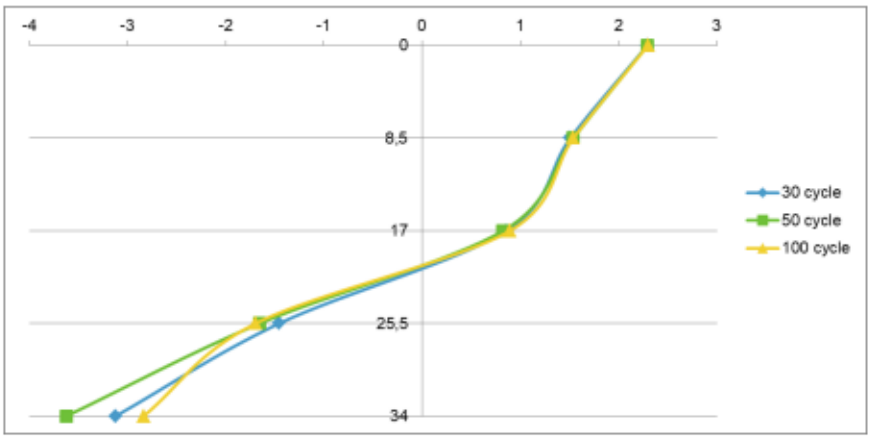

Figure 2.16. Displacement of mortar beam [12].

2.5. Arduino and Magnetometers

Equipment of the laboratory is one of the essential parts of experimental studies to record events and generate signals. Several types of equipment and software have been used and in most cases, they could be expensive. However many tasks do not need expensive software or equipment. In these cases, open-source hardware and software could be sufficient and affordable. Hence the popularity of microcontroller boards is increasing due to their affordable prices, ease of software writing, and community supports. Other advantages of the boards are acquiring data from sensors and switches, controlling motors, LEDs, etc. communication with other devices such as computers, cell phones, and even other boards [71].

Microcontroller boards generally have similar characteristics, though they have different processor architectures and programming languages. Arduino boards are one of the most popular microcontroller boards that are using engineering applications and the common Arduino boards are shown in Figure 2.17. Matteo et al. [72] proposed a study on the dam internal erosion detection system based on Arduino. Arduino boards also are used to control robotic equipment such as model helicopters [73] and in the laboratory [74]. Real-time monitoring of traffic flows [75], Wireless Control System

[76], and Water Vapour Diffusion Characteristics of Geomaterials [77] are examples of Arduino boards applications in civil engineering.

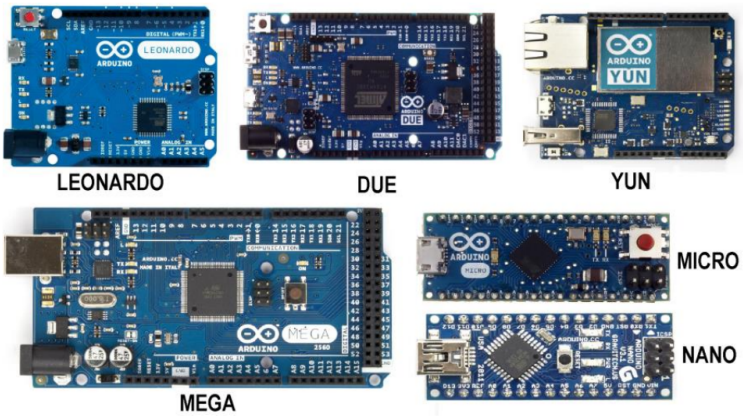

Figure 2.17. Popular Arduino boards [13].

The variety of Arduino compatible sensors extends applications of the boards. Temperature, humidity, distance, vibration, water level, microphone, and other digital and analog sensors can be used with Arduino boards. The magnetometer is another sensor to measure the magnetic field that a part of the applications in engineering [78] [79] [80].

3. METHODOLOGY

In this chapter, materials used in the tests, equipment, instrumentation, loading mechanism, and test conditions are outlined.

3.1. Materials

3.1.1. Model Pile

Segmental piles with variable flexural rigidity were used as model piles in this research. Model piles were produced referring to the project of Baykal et Al. (2014) [20] [11]. The piles comprise of mortar blocks, rubber pads, and steel wire. In order to form a pile, a steel wire as shown in Figure 3.1 is installed through mortar blocks and rubber pads. To adjust flexural rigidity, the steel wire was tensioned. Finally, the piles were obtained as shown in Figure 3.2, and pile dimensions are 320 mm x 50 mm x 50 mm.

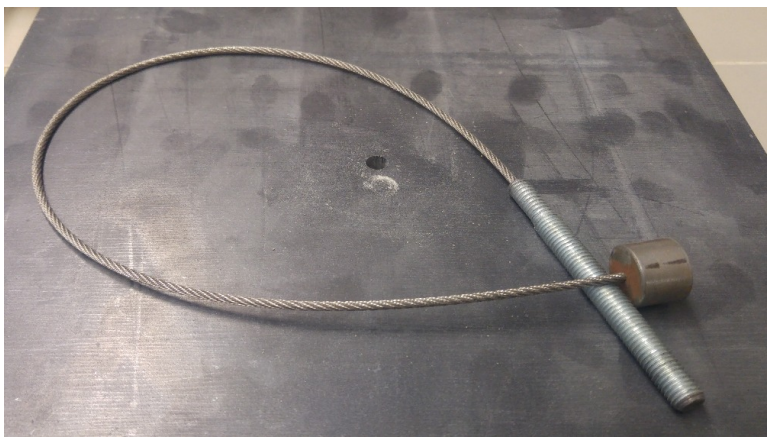

Figure 3.1. Steel cable.

Every component of the pile was ready for assembly, before loading of steel cable. In order to provide flexural rigidity to the pile, the steel wire was loaded with steel extrusion technique, before fixing of pile internal compressing load. Steel tension device with model pile in Figure 3.3.

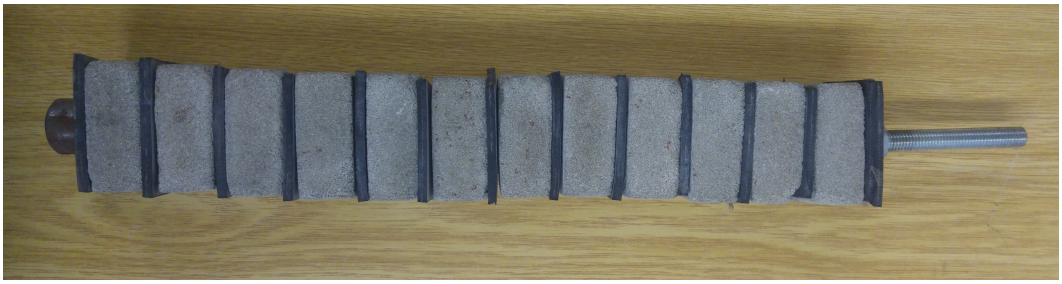

Figure 3.2. Model pile after assembling.

Figure 3.3. Steel tension test device.

3.1.1.1. Three Point Bending Test. Three-point bending tests were applied to measure the flexural stiffness of each pile based on ASTM D790-17. The three-point bending test is shown in Figure 3.5. Displacements and loads have been measured and with them, the flexural stiffness of each pile has been calculated. Three-Point Bending Test is shown in Figure 3.4.

Figure 3.4. Three point bending test device.

3.1.1.2. Mortar Blocks. Mortar blocks were needed to form a model pile. In this context, the produced mortar blocks were assembled to form a post-tension beam model pile. Confirming to the requirements of ASTM C270 [81], Portland Cement was used and the mix ratios for cement, water, and sand were 1, 0.5, and 3, by weight. A steel mold was used for the production of concrete blocks as shown in Figure 3.6. By

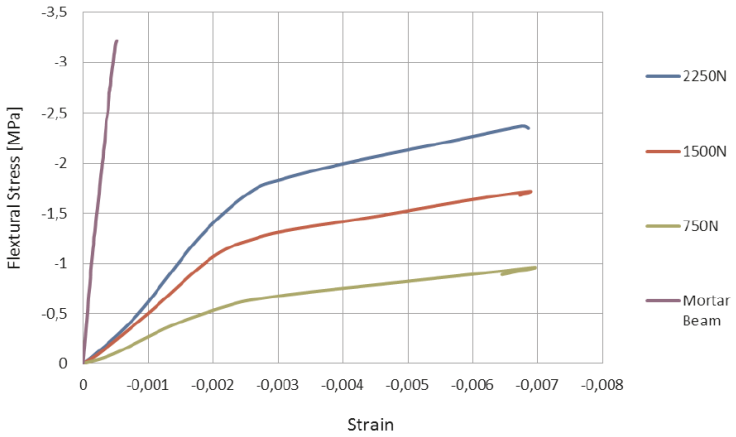

Figure 3.5. Stress strain curves of the SPVFR.

using this steel mold, mortar blocks were produced and they have width between 48 mm and 51 mm, height between 18 mm and 21.5 mm, and weight between 92.8 g and 109 g. The average compressive strength was obtained 20 MPa [11].

Figure 3.6. Steel mold.

3.1.1.3. Rubber Pads. Rubber shore 60 is a common type of rubber in industrial usage. In this research, shore 60 rubber was used as elastic rubber material in the production of the model pile. Rubber pads were placed between two mortar blocks. Shore 60 rubber used in this study has 3 mm thickness and other properties are listed in table 3.1. A mortar block and a shore 60 sheet are shown in Figure 3.7.

Table 3.1. Rubber properties details [11].

Rubber Type	Neoprene Rubber 1
General Description	Soft rubber
Style	7797
Colour	Black
Tensile Strength (KN/m2)	$10x10^3$
Elongation at Failure (%)	125
Elastic Modulus (MPa)	3
Thickness (t) (mm)	3
Rubber Shore (A)	60

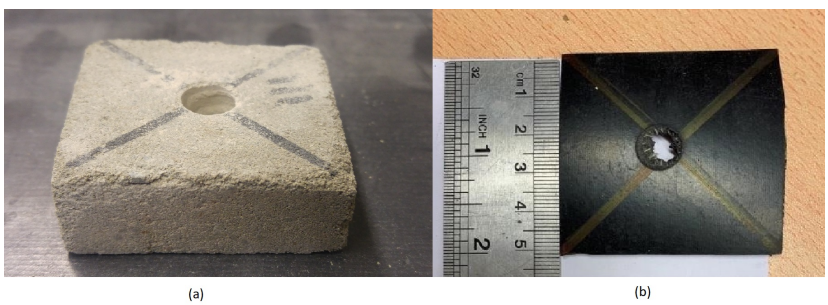

Figure 3.7. Mortar block (a) and Shore60 rubber (b).

3.1.2. Soil Material Properties

The fill material consisted of dry, clean, and coarse sand. According to ASTM 2487 [82], soil classified as poorly graded sand (SP). The particle size distribution of sand is shown in Figure 3.8. The soil has properties as C_c: 0.84, C_u: 2.41 and D_{50}: 2.00. The soil was placed in the test box after the pile placement for each experiment. To obtain target density for loose conditions, sand was placed without any compression. For the medium-dense conditions, sand was compressed at every layer placement.

Soil was

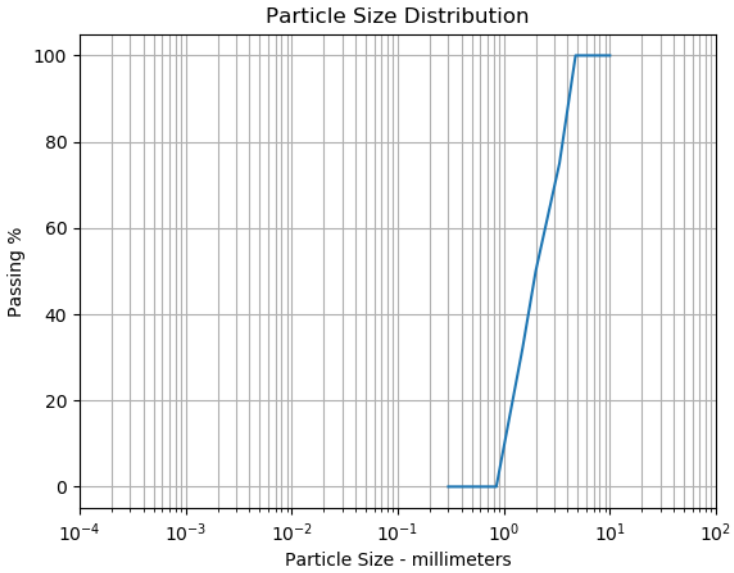

Figure 3.8. Grain size distribution of soil.

According to ASTM D4253, maximum and minimum densities were obtained as 15.40 kN/m^3 and 14.12 kN/m^3, respectively. The maximum and minimum void ratios of soil were obtained as 0.55 and 0.65, respectively. Results of direct shear tests show that friction angles of soil in loose and dense states are 39.5 and 42.8 degrees, respectively. Physical properties of sand are shown in Table 3.2.

Table 3.2. Sand properties.

10 percentile grain diameter, D_{10} [mm]	1.02
30 percentile grain diameter,D_{30} [mm],	1.47
60 percentile grain diameter, D_{60} [mm]	2.41
Uniformity Coefficient, C_u	2.41
Coefficient of Curvature, C_c	0.84
Minimum dry unit weight [kN/m^3]	14.12
Maximum dry unit weight [kN/m^3]	15.40
Minimum void ratio, e_{min}	0.55
Maximum void ratio, e_{max}	0.65
Friction angle (Loose), ϕ [°]	39.5
Friction angle (Dense), ϕ [°]	42.8

3.2. Test Box and Loading Mechanism

Large size-large displacement direct shear device [70] was used in this research as test box and loading mechanism. The Interior length, height, and width of the lower box are 900 x 400 x 300 mm, and the interior length, height, and width of the upper box are 300 x 200 x 300 mm, respectively. The upper and lower boxes of the device are shown in Figure 3.9. The test box has two parts, the lower part was used for the soil model and the upper part that has not been filled with soil was used only to transfer the lateral load to the pile head and fixing the pile head.

The shear device has three loading mechanisms. The first one is a horizontal displacement control system with a linear step motor and this loading mechanism was used to load pile head laterally in this research. Static load is created by a linear step motor with constant strain. The load was applied as 1 mm per minute and cyclic loads are also possible. The other one is an antagonistic-cyclic loading system with pneumatic artificial muscles. The third one is the normal loading with pneumatic artificial muscles.

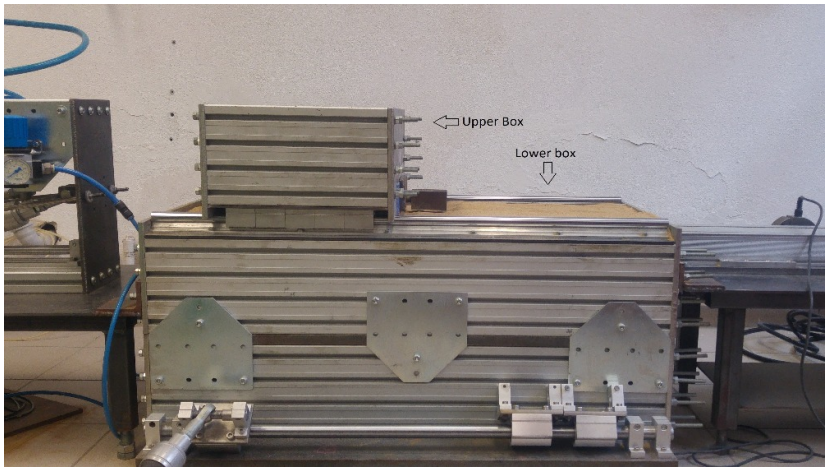

Figure 3.9. Test box.

As shown in Figure 3.10, the model piles were placed. The Lower box was filled with soil and the piles were placed in the lower box. The upper box of the device was used to transfer the lateral load. The upper box was free to move laterally. The lateral load was measured with a load cell assembled between the upper box and the linear step motor. The model pile in the test box is shown in Figure 3.11.

Figure 3.10. Scheme of test.

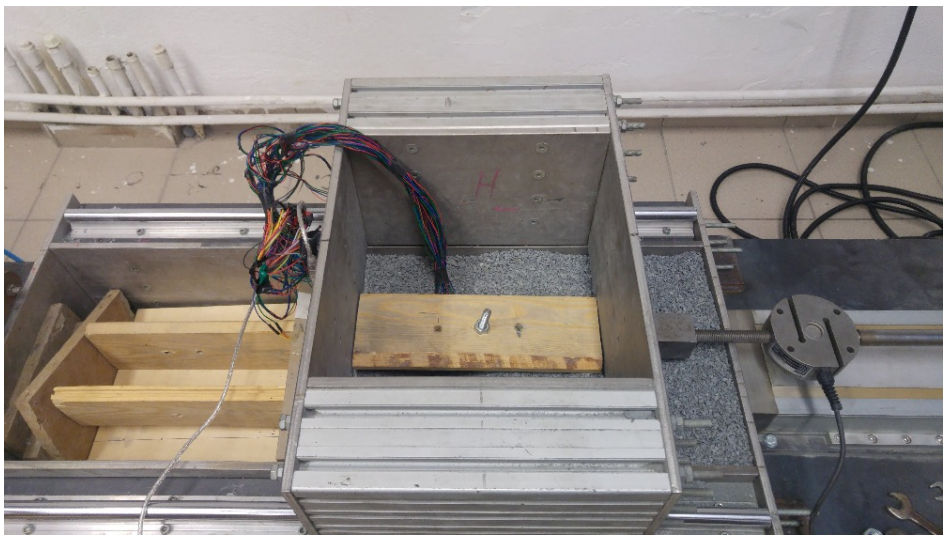

Figure 3.11. The pile in the test box.

3.3. Instrumentation

3.3.1. Arduino

Arduino modules refer to microcontroller-based development boards which are open-source prototyping platforms. Arduino UNO development board is shown in Figure 3.12. In this study, an Arduino board was used as a data acquisition system and a power supply to sensors. Arduino board was programmed to decide how and how often the data from sensors will be received. To provide it, as a standard procedure, the Arduino board was programmed and compiled code was uploaded to the Arduino board by using Arduino IDE software that is shown in Figure 3.13.

Since microcontrollers work with common data formats such as Intel 8-bit hex file format that is one of the most popular file formats, programs coded in relatively low-level programming languages such as C/C++ or Java and complies with these file formats. [83]. Arduino IDE software has been developing by Arduino Community and one of the main objectives is the simplification of programming with the simplified syntax of C/C++ languages. Another objective of this software is to upload compiled code to Arduino boards or direct microcontrollers.

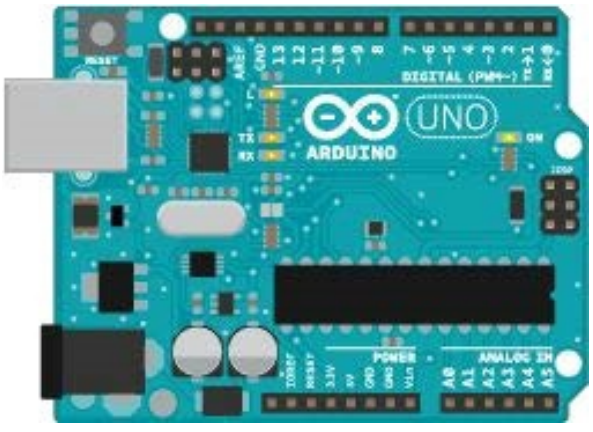

Figure 3.12. Arduino Uno development board.

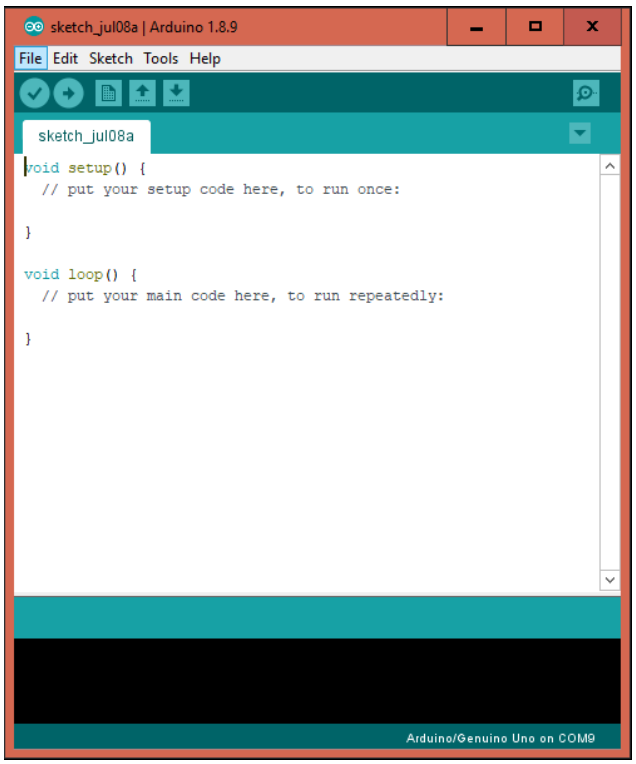

Figure 3.13. Arduino IDE software.

3.3.2. Magnetometers

Three-axis magnetometers are sensors that provide both the direction and magnitude of the magnetic field data in digital format. Since they are light-weight, having low-power requirements, and reliable, three-axis magnetometers are advantageous [84]. Three-axis magnetometer is shown in Figure 3.14. In this study, the segmental pile was used as a model pile that is presented in section 3.1.1 and relative inclinations of these segments were investigated. The result of the investigation, the pile movement pattern was modeled. With measuring the pile segment angles, pile lateral displacements were attempted to be calculated. Three-axis magnetometers were used to obtain inclinations of each segment. In order to provide this, 12 magnetometers were assembled. Sensors locations are shown in Figure 3.16 and assembling of sensors is shown in Figure 3.15.

HMC5583L sensors that are three-axis magnetometers produced by Honeywell were used in this research. Three-axis magnetometers need calibration to obtain precise

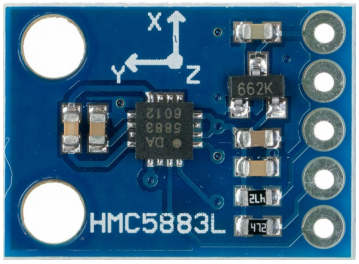

Figure 3.14. HMC5883L 3 axis magnetometer.

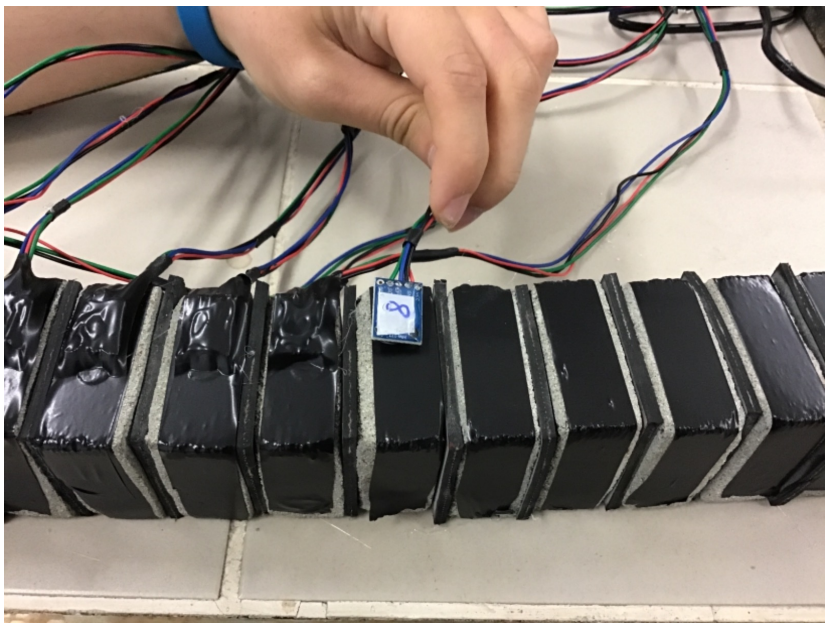

Figure 3.15. Assembling of sensors.

values [14] because of drift and biases. In order to calibrate each sensor, bias, and gain matrices for each sensor should be created [84]. After subtracting bias values and multiplication transformation matrix, three-axis values can be used for measurement. Calibration equation is shown in Equation (3.1).

$$\begin{pmatrix} C_x \\ C_y \\ C_z \end{pmatrix} = \begin{bmatrix} \alpha_{11} & \alpha_{12} & \alpha_{13} \\ \alpha_{21} & \alpha_{22} & \alpha_{23} \\ \alpha_{31} & \alpha_{32} & \alpha_{33} \end{bmatrix} X \begin{pmatrix} Raw_x - \beta_x \\ Raw_y - \beta_y \\ Raw_z - \beta_z \end{pmatrix} \tag{3.1}$$

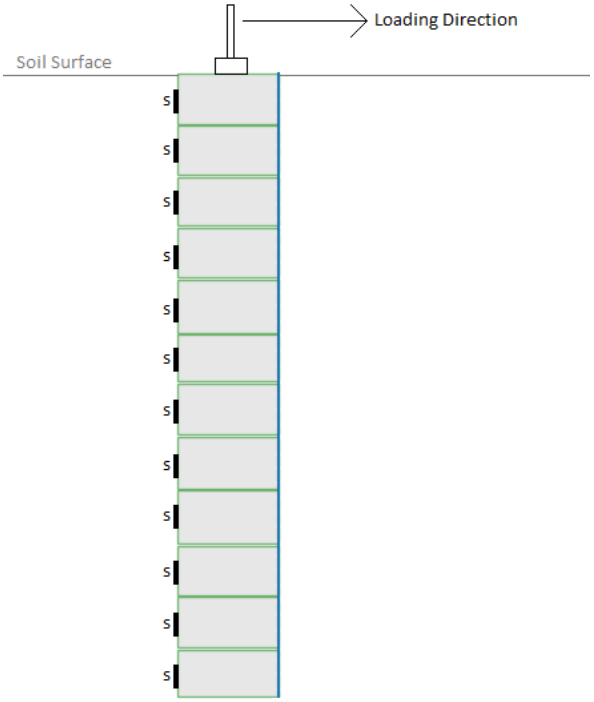

Figure 3.16. Locations of magnetometers on pile.

In order to estimate bias and transformation matrices, parametric equation of an ellipsoid, α values and β values are obtained using Equation (3.2) [14]. The calibration procedure continues until measurements cover most of the surface of an ellipsoid. In this research 12 measurements were used to cover ellipsoid and for calculations an open-source software named Magmaster version 1.0 was used.

$$H^2 = ((V_x(t) - \beta_x)/\alpha_x)^2 + ((V_y(t) - \beta_y)/\alpha_y)^2 + ((V_z(t) - \beta_z)/\alpha_z)^2 \qquad (3.2)$$

HMC5883L sensors use I2C protocol on Arduino board. Therefore more than one sensor can be used with one arduino but each sensor has to have different hexadecimal addresses. Because all HMC5583L sensors have the same addresses, to overcome this problem I2C multiplexers were used. With this method, data from sensors could be obtained with one arduino board. I2C multiplexer is shown in Figure 3.18.

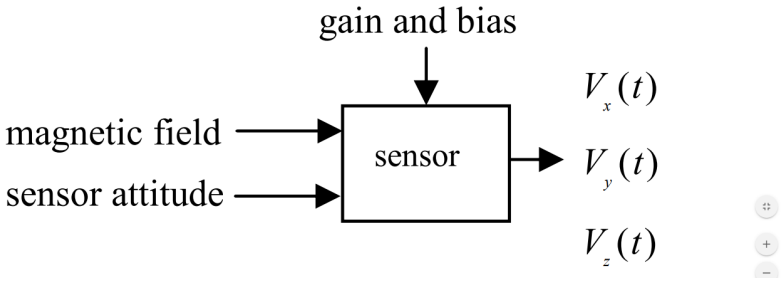

Figure 3.17. Representation of sensor [14].

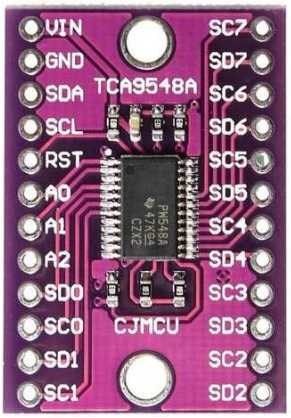

Figure 3.18. I2C multiplexer.

3.3.3. Processing and Controlling of Instrumentation

3.3.3.1. Processing of Raw Data. Block inclinations were processed with an algorithm that was coded in Python programming language in order to calculate lateral displacements of blocks. Python was preferred in this study because of simplicity. The flowchart of the code is shown in Figure 3.19. For calculations, Numpy and illustrations, Matplotlib modules of Python were used.

3.3.3.2. Testing of Equipment. As mentioned before, to overcome observing problem of pile movement in the soil, the inclination values were used to calculate the lateral displacement of the pile through pile length. Since this method has not been used and tested yet, the method was tested in the same condition by control tests.

The instrumented pile has been placed in the large size-large displacement direct shear testing device without soil and initial values have been measured. After that, the pile angle has been set 7.5 degrees as Figure 3.21 and calculated angles of pile blocks have been obtained from raw values of magnetometers and shown at Table 3.3. As shown in Table 3.3.

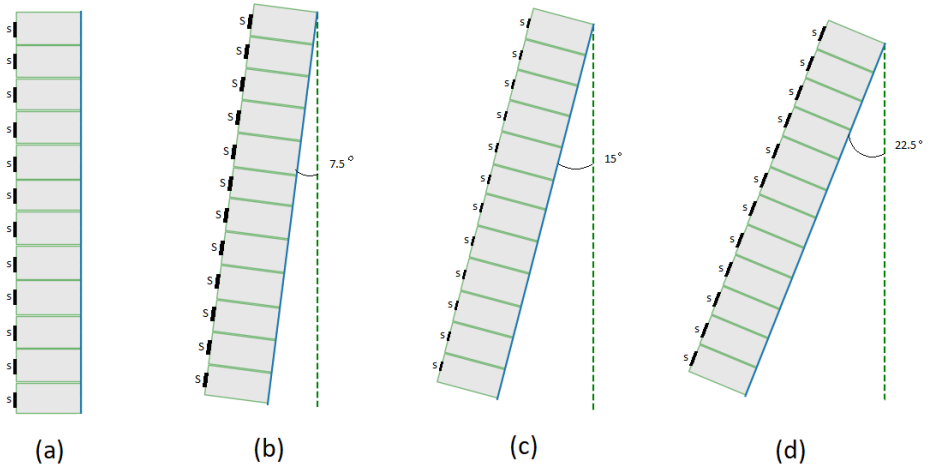

Figure 3.21. The pile position of control tests.

Table 3.3. Control test for 7.5°.

Block	**Test 1**	**Test 2**	**Test 3**
1	7.95	8.34	8.38
2	8.03	8.34	7.89
3	7.86	7.97	7.78
4	8.45	8.76	8.28
5	7.34	7.43	7.68
6	7.72 3	7.45	7.84
7	7.35	7.45	7.34
8	7.51	7.88	7.87
9	7.77	7.03	7.49
10	8.05	7.94	8.07
11	7.17	7.61	7.67
12	8.00	7.84	8.32
Mean	7.77	7.84	7.88

The pile angle has been set 15 degrees as shown in Figure 3.21 and calculated angles are shown in Table 3.4.

Pile angle has been set 22.5 degrees as shown in Figure 3.21 and calculated angles are shown in Table 3.5.

Standard deviation and mean values of control tests are given in Table 3.6 and control test results are given in Figure 3.22. The standard deviation for 7.5° is 0.39°, at 15° is 0.61°, and for 22.5° is 1.77°. Mean values are 7.83°, 14.37°, and 21.24° for 7.5, 15, and 22.5°, respectively. For the first four blocks mean standard deviation is 0.117, for the second four blocks is 0.16, and for the last four blocks is 0.24 for 7.5° inclination test. According to these values, the ferromagnetic metal parts of the segmental pile affects magnetometer measurement.

Table 3.4. Control test for 15°.

Block	**Test 1**	**Test 2**	**Test 3**
1	14.62	14.81	14.58
2	13.66	14.23	14.3
3	14.87	14.79	14.92
4	15.22	15.12	15.24
5	14.03	13.53	14.29
6	14.77	14.57	14.92
7	13.80	13.33	14.30
8	14.06	13.46	14.04
9	15.21	15.05	15.51
10	14.17	14.42	14.96
11	13.34	13.36	14.31
12	13.63	13.78	14.29
Mean	14.28	14.20	14.52

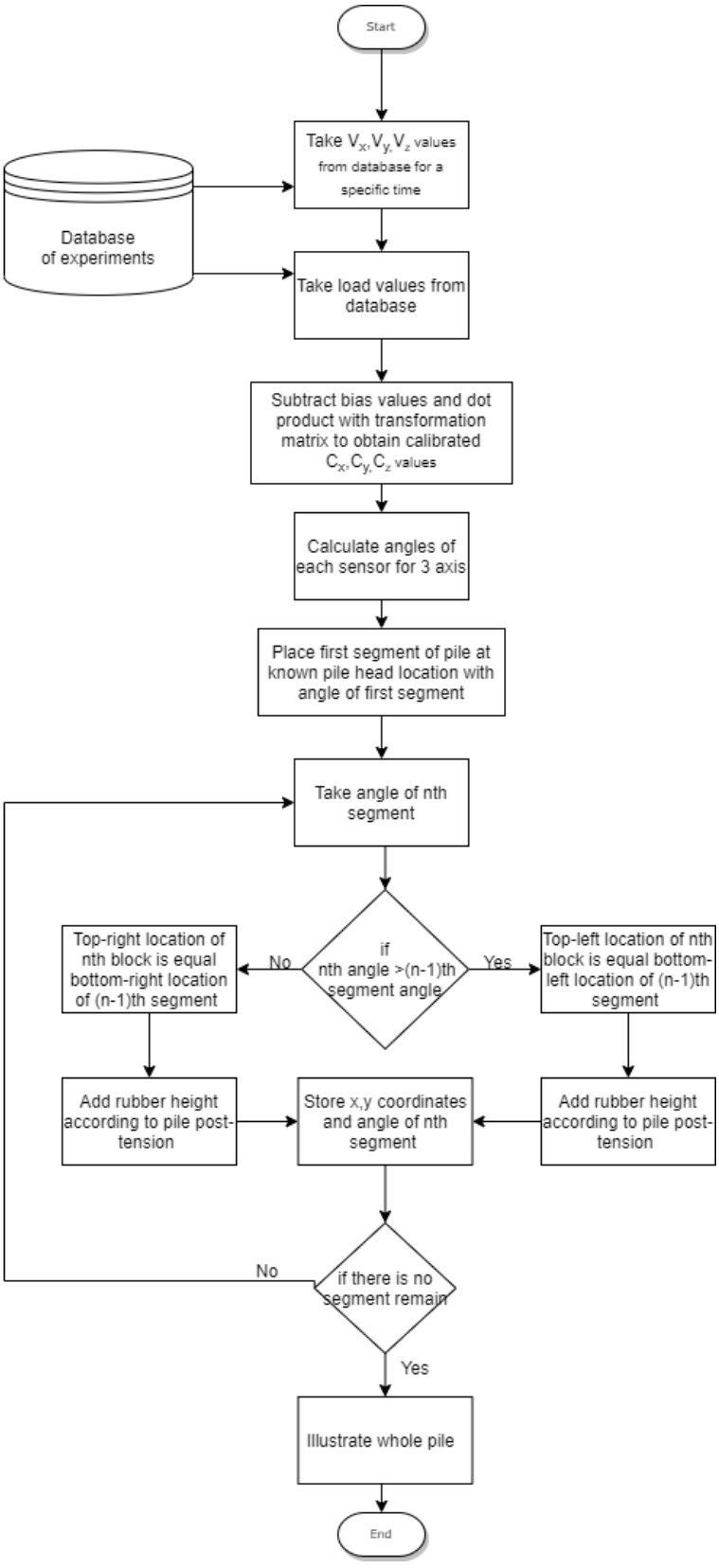

Figure 3.19. Flowchart of the code.

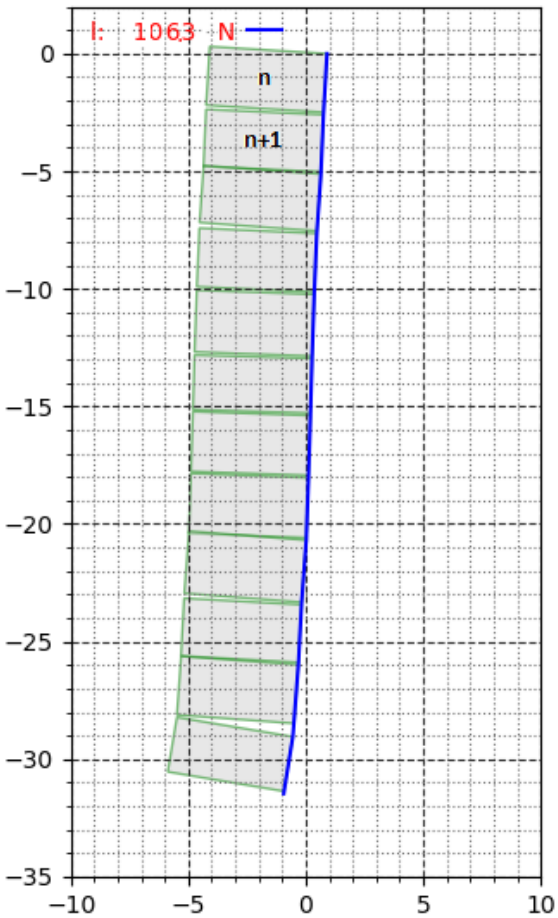

Figure 3.20. Example result of code.

Table 3.5. Control test for 22.5°.

Block	**Test 1**	**Test 2**	**Test 3**
1	22.84	22.36	22.35
2	19.54	20.22	19.99
3	22.03	23.06	21.57
4	22.08	22.80	21.98
5	21.60	23.59	21.74
6	23.12	24.56	23.03
7	20.11	19.66	19.84
8	19.60	19.96	19.66
9	22.61	22.00	22.49
10	19.06	18.65	18.89
11	18.55	18.05	18.48
12	22.66	23.58	22.31
Mean	21.15	21.54	21.03

Table 3.6. Standard deviation values of control tests.

Inclination	**7.5°**	**15°**	**22.5°**
Test 1	0.36°	0.64°	1.66°
Test 2	0.48°	0.68°	2.14°
Test 3	0.33°	0.46°	1.56°
Test 1,2,3	0.39°	0.61°	1.77°
Mean	7.83°	14.37°	21.24°

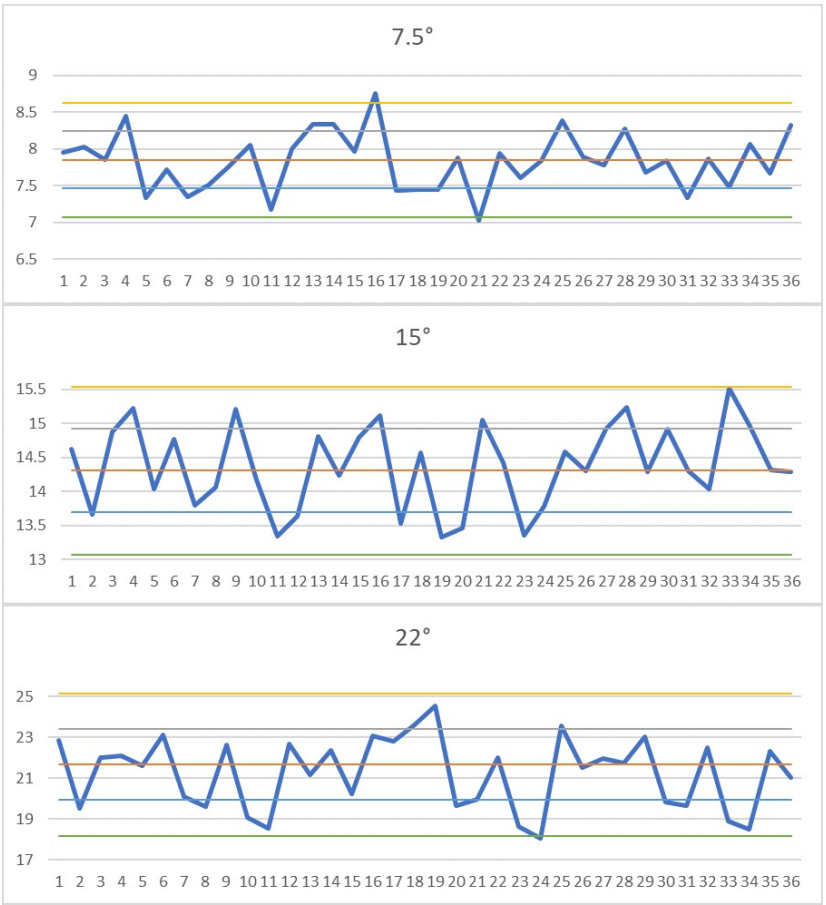

Figure 3.22. Results of the control tests.

3.4. Testing Conditions

In this research, two model piles were used and they had different flexural rigidities. These piles have post-tension load 750 N and 2250 N, respectively. Also, sand with loose and medium dense relative densities was used. The experiments and the test conditions. Experiments and conditions are listed in Table 3.7.

Table 3.7. The list of experiments.

Exp.	**Post-tention**	**Relative Density**	$\mathbf{K_{rc}}$	**EI ($\mathbf{Nm^2}$)**	$\mathbf{E_p/E_s}$
1	750 N	Loose (30%)	$2.1x10^{-3}$	29.3	42
2	750 N	Loose (30%)	$2.1x10^{-3}$	29.3	42
3	750 N	Loose (30%)	$2.1x10^{-3}$	29.3	42
4	750 N	Medium-Dense (60%)	$1.1x10^{-3}$	29.3	22
5	750 N	Medium-Dense (60%)	$1.1x10^{-3}$	29.3	22
6	750 N	Medium-Dense (60%)	$1.1x10^{-3}$	29.3	22
7	2250 N	Loose (30%)	$5.7x10^{-3}$	80.1	116
8	2250 N	Loose (30%)	$5.7x10^{-3}$	80.1	116
9	2250 N	Loose (30%)	$5.7x10^{-3}$	80.1	116
10	2250 N	Medium-Dense (60%)	$3.0x10^{-3}$	80.1	61
11	2250 N	Medium-Dense (60%)	$3.0x10^{-3}$	80.1	61
12	2250 N	Medium-Dense (60%)	$3.0x10^{-3}$	80.1	61

4. RESULTS

In this chapter, data obtained from the tests are presented. Laterally loaded pile experiments that are defined in the previous chapter are divided into sections based on the pile types and the soil densities. Respectively 750N pile in loose sand, 750N pile in medium-dense sand, 2250N pile in loose sand, and 2250N pile in medium-dense sand are presented in Chapter 4.2 - Chapter 4.5. Experiments are listed in Table 3.7.

4.1. Load-displacement Curves

Horizontal load and lateral displacement of the pile head were measured during the experiments. Figure 4.1 represents the load-displacement behavior of the experiments grouped by experiments.

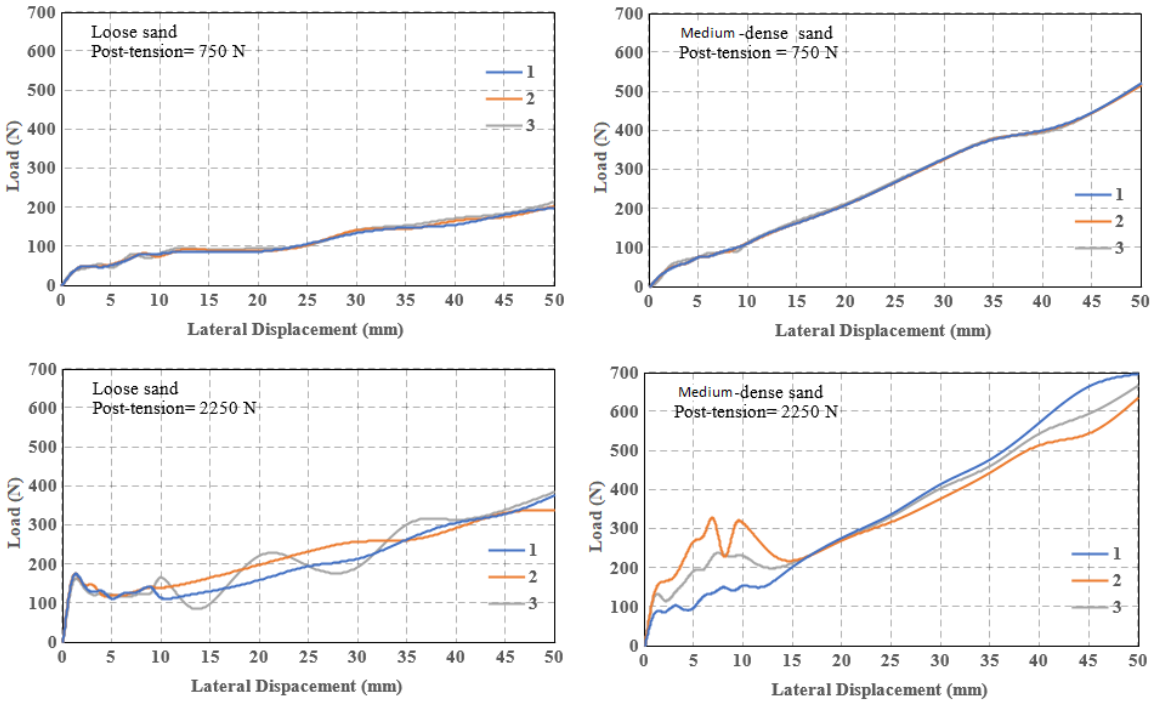

Figure 4.1. Load-displacement curves of experiments.

The pile displacement curves for the 2250N segmental piles in loose and medium dense sand show differences for three repetitions. The general trend for both cases is the immediate mobilization of resistance at small displacements like 1 or 2 mm reaching more than 100 N. Three tests for the loose condition show similar trend up to 10 mm displacement and fluctuation was observed beyond this value with a narrow band. For medium dense cases though a large fluctuation is observed between 2mm and 15 mm displacements. Beyond this displacement, the fluctuation diminishes. The fluctuation is not observed for all cases with 750 N pile. The higher flexural rigidity of 2250N pile may have led to this behavior. The dilation behavior of the sand has not been studied in detail so no further explanation will be attempted.

4.2. Overview of Experiments

In order to compare the experiments, the pile head loads for 4, 12, 25, and 50 mm pile head displacement are given in Figure 4.2. With a quick review, with lateral head displacement, the pile resistance increases gradually for all conditions. At the beginning of the experiments, the pile with 2250 N post-tension showed a significantly higher capacity than 750 N. With increase displacement 750 N capacity reached 55 % of the 2250 N pile. However, with the increase of the displacement, soil density affects the required pile head load. Both 750 and 2250 N piles in medium-dense soil required more pile head load to displace than the piles in loose soil.

The pile displacement values with depth of the pile with 750 N post-tension in loose sand is given Figure 4.3. The pile behaved flexible pile with plastic hinge development. The pile displacement values with depth of the pile with 750 N post-tension in medium-dense sand is given Figure 4.4. The pile behaved as flexible pile with a bending point. The pile displacement values with depth of the pile with 2250 N post-tension in loose sand is given Figure 4.5. The pile behaved as rigid. With the increase of displacement, the bending behavior was disappeared. The pile displacement values with the depth of the pile with 2250 N post-tension in medium-dense sand is given Figure 4.6. The plastic hinge is presented and the pile behaved as flexible pile. For 2 condition, K_{rc} values are also in the similar range.

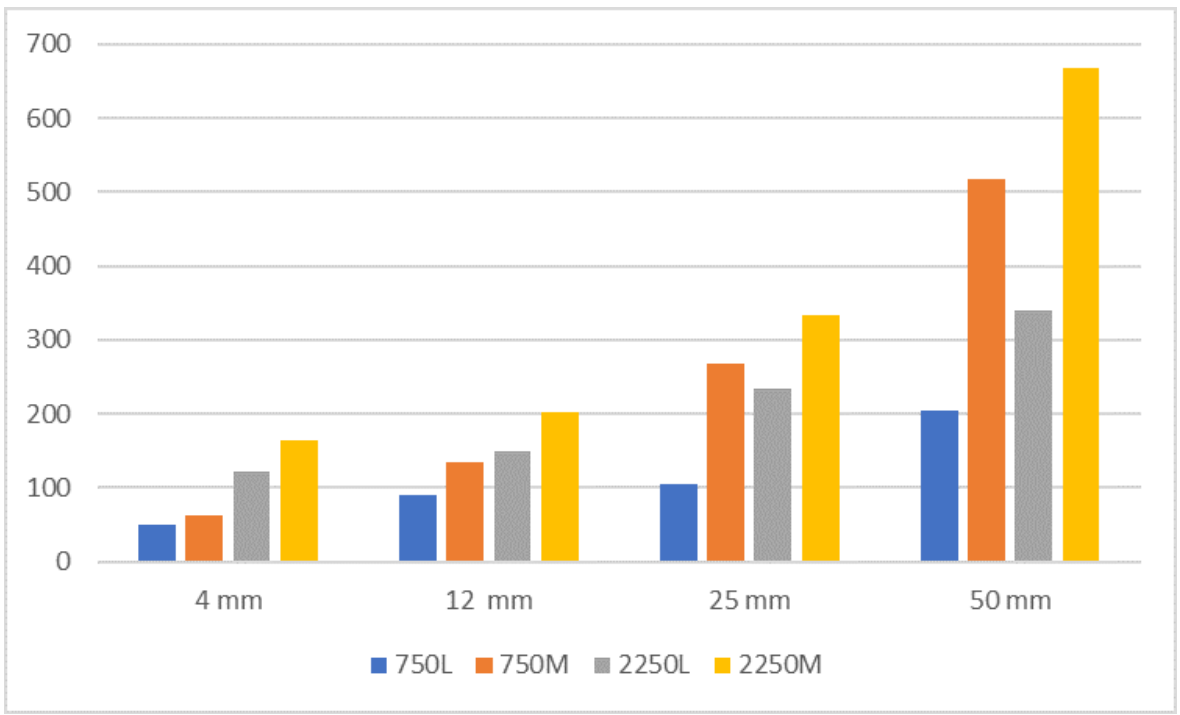

Figure 4.2. Pile head load with 4, 12, 25, and 50 mm displacement.

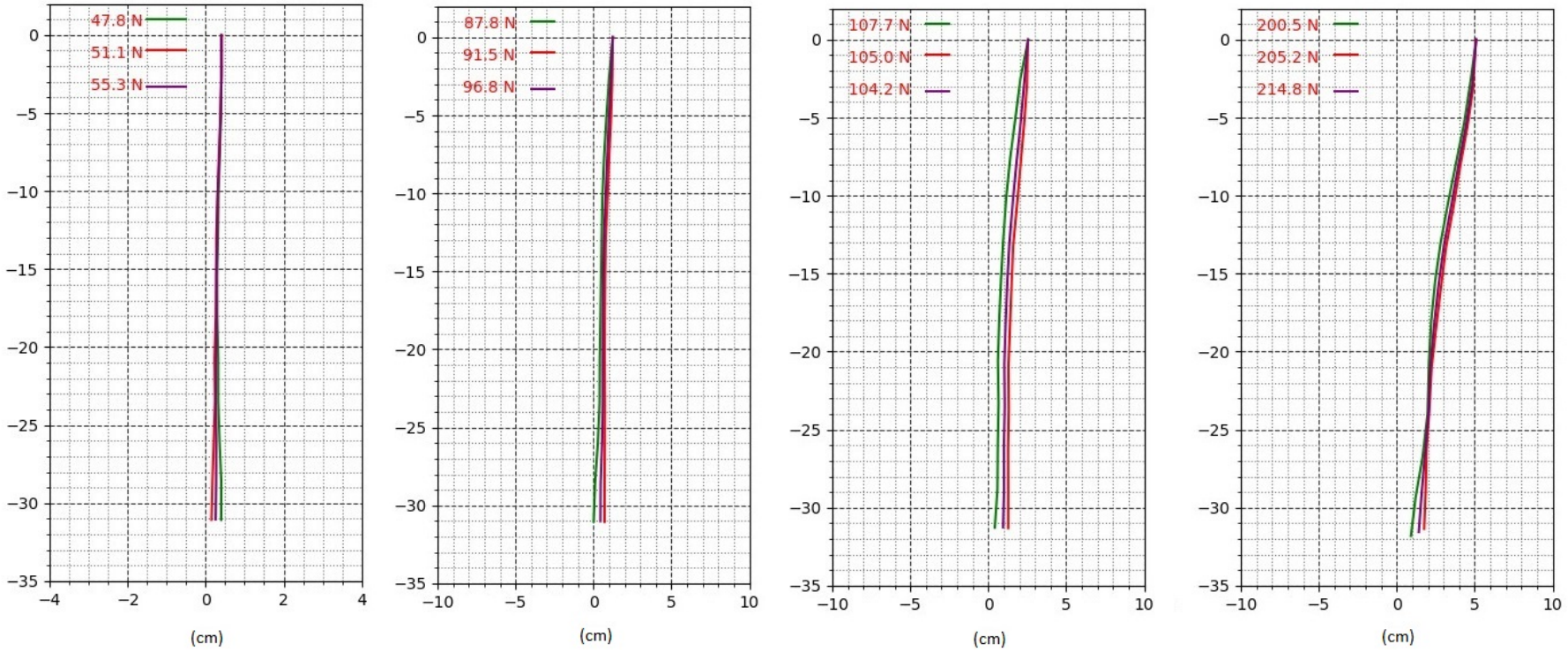

Figure 4.3. 750N pile in loose sand with 4, 12, 25, and 50 mm displacement.

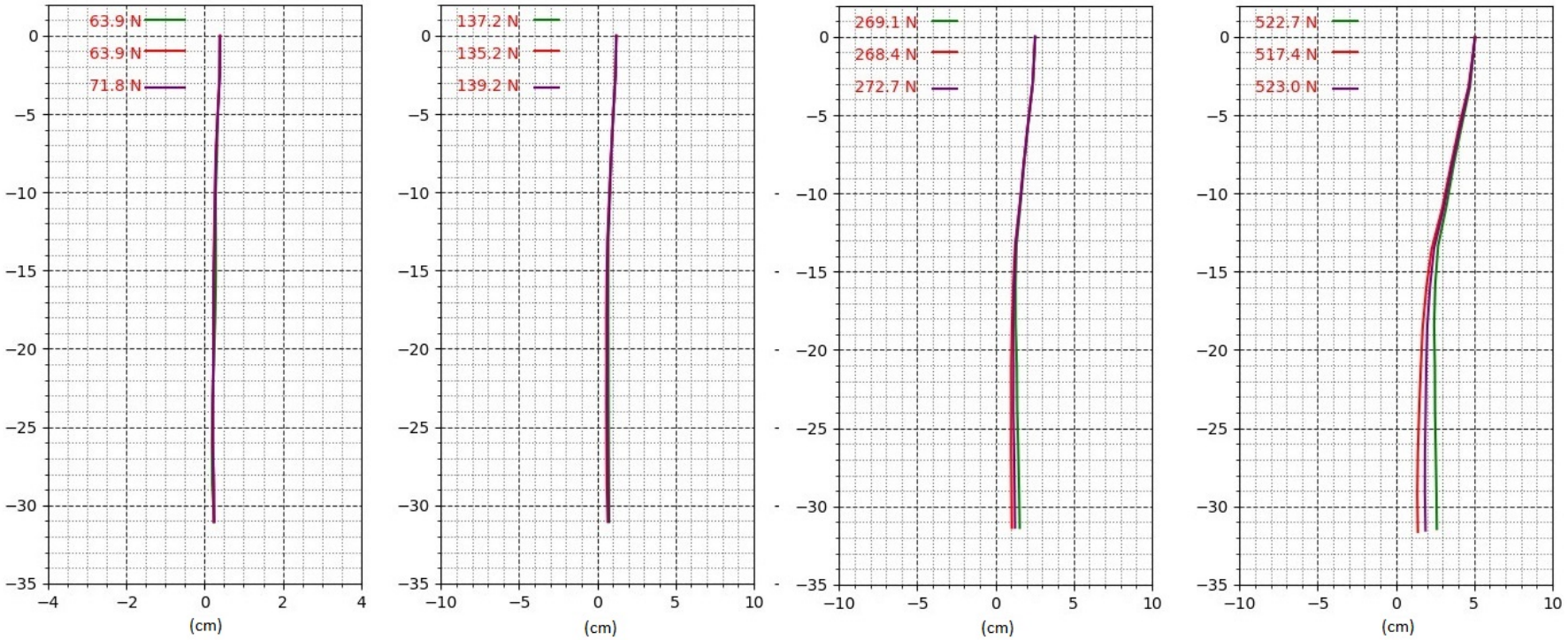

Figure 4.4. 750N pile in medium-dense sand with 4, 12, 25, and 50 mm displacement.

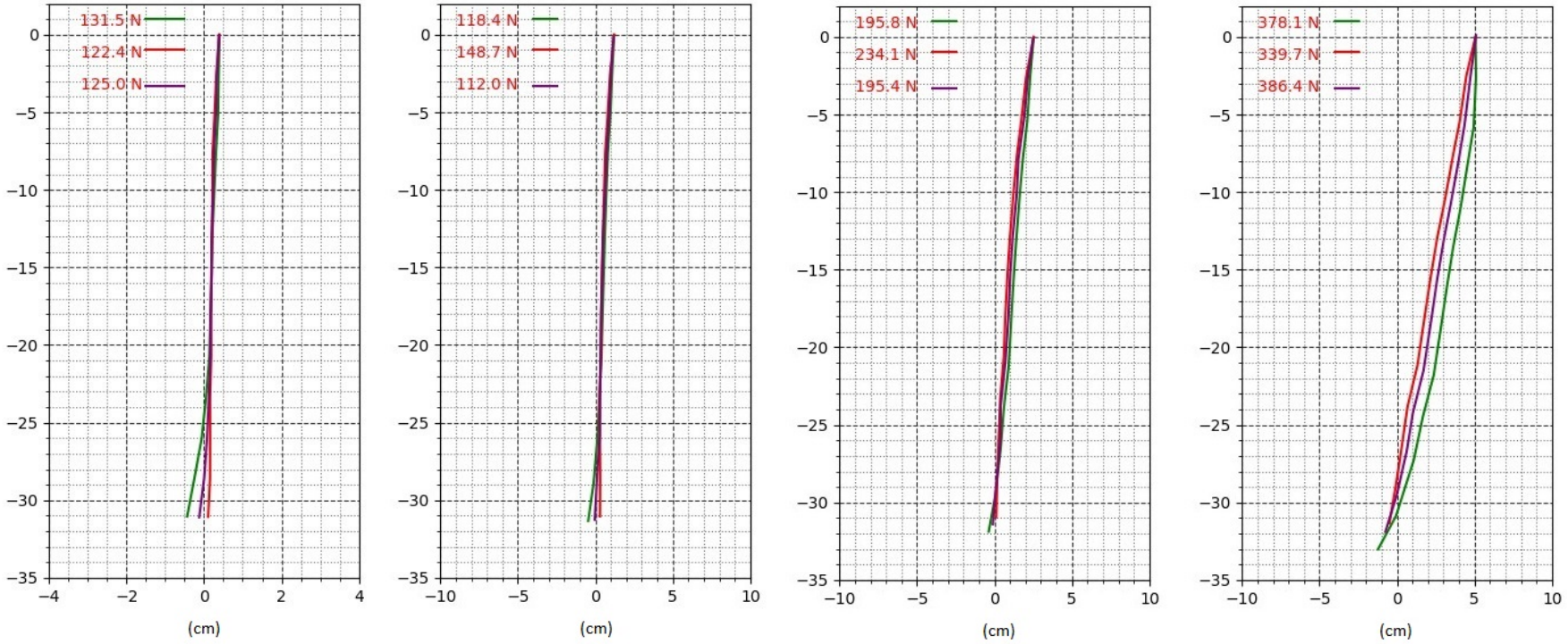

Figure 4.5. 2250N pile in Loose Sand with 4, 12, 25, and 50 mm displacement.

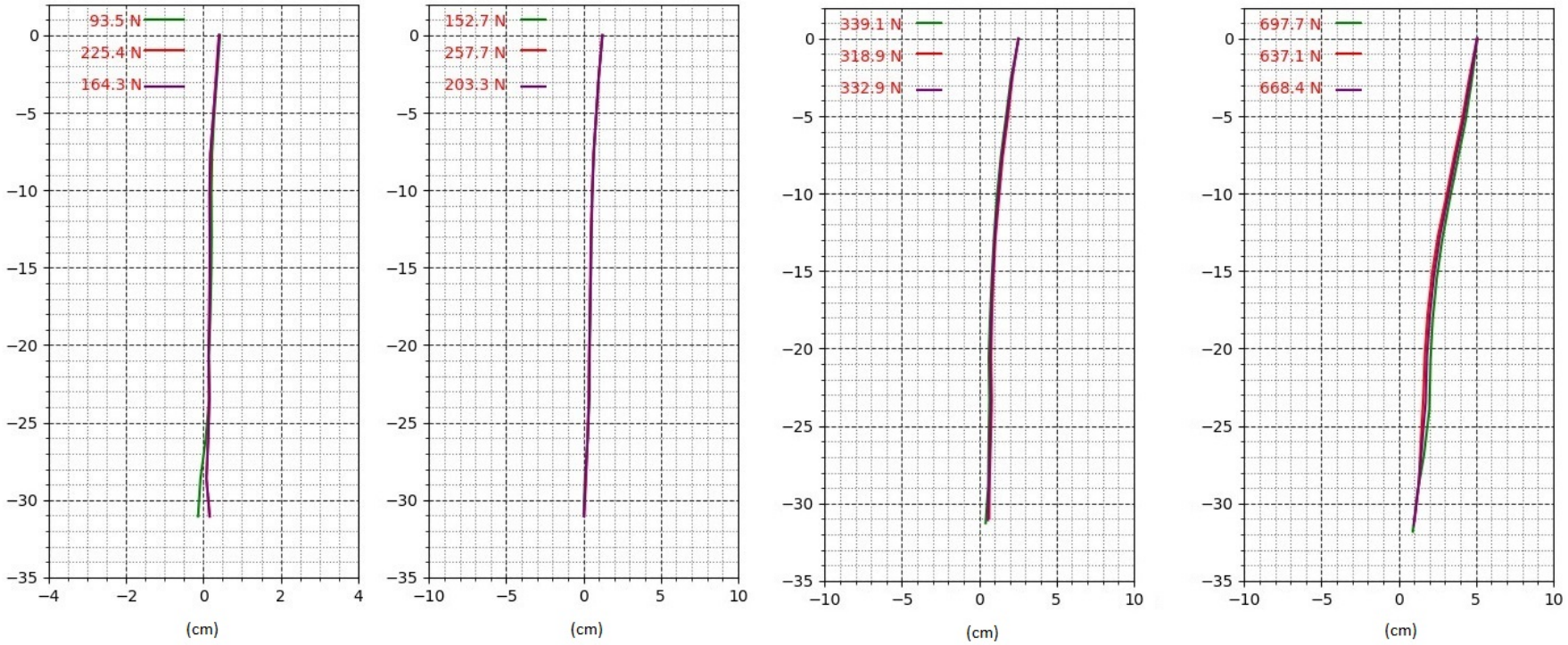

Figure 4.6. 2250N pile in medium-dense sand with 4, 12, 25, and 50 mm displacement.

4.3. Rotations of Blocks

Since the inclinations of blocks were measured with three-axis magnetometers, it is possible to measure rotations of blocks around the steel wire with the same process. Rotations of pile blocks for 750 N pile in loose sand are shown in Table 4.1. As the lateral displacement increases some of the blocks rotate and these rotations may reach up to 14 degrees at block numbers 3,4 and 5. These are large rotations and for monolithic concrete pile, these values may be very critical.

Table 4.1. Rotations of blocks versus head-displacements for 750 N pile in loose sand.

Block	**10 mm**	**20 mm**	**30 mm**	**40 mm**	**50 mm**
1	-0.35°	-1.0°	-1.46°	-2.19°	-2.26°
2	1.73°	3.16°	4.36°	6.47°	7.4°
3	2.97°	5.61°	8.26°	10.73°	12.68
4	2.54°	5.94°	8.25°	10.66°	12.83°
5	3.09°	6.2°	8.32°	11.54°	13.83°
6	0.61°	1.89°	3.76°	6.23°	7.74°
7	0.22°	1.35°	2.54	4.03°	5.54°
8	-0.16°	0.82°	1.33°	1.84°	3.35°
9	-0.06°	1.62°	2.44°	4.54°	4.21°
10	-0.53°	0.22°	0.32°	0.84°	2.3°
11	-0.98°	-0.38°	-0.68°	-0.16°	1.26°
12	-2.82°	-1.5°	5.61°	7.68°	10.56°

Rotations of pile blocks for 750 N pile in medium-dense sand are shown in Table 4.2. As the lateral displacement increases some of the blocks rotate and these rotations may reach up to 17 degrees at block numbers 3,4 and 5. These blocks are around the bending point. Therefore, it could be related to the bending movement of the pile.

Table 4.2. Rotations of blocks versus head-displacements for 750 N pile in medium-dense sand.

Block	**10 mm**	**20 mm**	**30 mm**	**40 mm**	**50 mm**
1	-0.35°	-0.99°	-1.79°	-1.82°	-1.6°
2	2.79°	5.83°	8.15°	10.2°	13.43°
3	3.53°	7.4°	10.44°	13.81°	17.35°
4	2.62°	5.59°	8.26°	11.31°	15.06°
5	1.36°	5.64°	9.03°	12.4°	18.35°
6	-0.23°	0.54°	2.0°	2.52°	5.24°
7	-0.11°	-0.09°	0.32°	0.1°	2.07°
8	0.01°	-0.72°	-1.35°	-2.32°	-1.09°
9	0.26°	0.38°	0.74°	1.01°	2.34°
10	-0.15°	-0.36°	-1.17°	-1.62°	-1.18°
11	-0.31°	0°	-1.0°	-0.92°	-1.28°
12	-2.27°	-2.9°	1.78°	2.31°	6.48°

Rotations of pile blocks for 2250 N pile in loose sand are shown in Table 4.3. In this condition, the pile behaves as a rigid pile. Therefore, unlike other conditions, rotations of blocks were not concentrated at the special points of the pile.

Table 4.3. Rotations of blocks versus head-displacements for 2250 N pile in loose sand.

Block	**10 mm**	**20 mm**	**30 mm**	**40 mm**	**50 mm**
1	5.7°	12.19°	14.19°	13.14°	12.58°
2	3.7°	7.46°	9.4°	10.32°	10.97°
3	5.42°	10.37°	13.12°	15.38°	17.27°
4	2.91°	6.82°	9.87°	13.42°	15.7°
5	2.14°	5.95°	8.13°	12.39°	14.02°
6	1.73°	3.65°	6.56°	8.99°	11.5°
7	1.87°	3.09°	5.74°	7.56°	9.8°
8	2.01°	2.53°	4.92°	6.14°	8.26°
9	3.28°	4.53°	6.32°	8.77°	10.91°
10	2.04°	8.7°	14.03°	18.36°	22.99°
11	3.77°	4.15°	6.18°	9.47°	11.10°
12	2.14°	3.3°	4.11°	0.76°	1.01°

Rotations of pile blocks for 2250 N pile in medium-dense sand are shown in Table 4.4. Like 750 N pile also in this condition, because of the pile bending behavior rotations were concentrated around the bending point. The rotations are much larger for 2250 N pile and for medium dense case the top block rotate significantly even at 10 and 20 mm displacements. This is why large fluctuations are observed in the lateral head load.

Table 4.4. Rotations of blocks versus head-displacements for 2250 N pile in medium-dense sand.

Block	**10 mm**	**20 mm**	**30 mm**	**40 mm**	**50 mm**
1	7.6°	18.66°	28.18°	14.31°	7.16°
2	6.6°	12.66°	16.55°	18.4°	19.41°
3	5.94°	11.09°	16.27°	20.64°	21.6°
4	3.35°	7.3°	12.92°	17.31°	19.32°
5	1.01°	3.98°	8.27°	12.45°	14.91°
6	1.55°	2.85°	5.33°	8.59°	9.96°
7	1.31°	2.375°	3.56°	5.59°	6.6°
8	1.07°	1.9°	1.79°	2.94°	3.24°
9	0.38°	-0.26°	-0.32°	-0.25°	0.58°
10	0.1°	0.33°	0.985°	2.19°	2.68°
11	-0.87°	-1.23°	0.18°	1.44°	2.13°
12	1.27°	-0.54°	0.44°	1.6°	3.05°

5. DISCUSSION

The discussion presented below is limited to completed experiments. Verification tests with control monolithic concrete pile were not conducted due to pandemic restrictions. The horizontal displacement values along the pile except the pile head are also not verified with direct measurement. The displacement values are derived from the magnetometer measurements placed on each block.

5.1. Effect of Soil Stiffness

To compare the effect of relative density on pile behavior under laterally loading, the piles with 750 and 2250 N post-tension results in two different soil density were compared.

5.1.1. 750N Pile in Loose and Medium-Dense Sand

The pile displacement values are presented for 10, 25, 35, and 50 mm pile head displacement for loose and medium dense sand in Figures 5.1 and 5.2. For 750 N segmental pile E_p/E_s for loose state is 42 and for the dense state the modulus ratio is 22. The ratio of pile capacity for pile installed in medium dense sand and loose sand varies between 1.49 and 2.52 for 10 mm and 50 mm displacement respectively. The E_p/E_s ratio for 750 N pile in medium dense sand is 0.52 of the E_p/E_s ratio in loose sand. Head load values and ratios are given in Table 5.1.

5.1.2. 2250N Pile in Loose and Medium-Dense Sand

The pile displacement values are presented for 10, 25, 35, and 50 mm pile head displacement for loose and medium dense sand in Figures 5.3 and 5.4. The pile lateral capacity ratio for 2250N pile installed in medium dense to that of loose sand decreases from 2.75 to 1.68 for 10 mm and 50 mm displacement, respectively. The capacity ratio of the pile increases with lateral displacement for medium dense sand for 750 N pile.

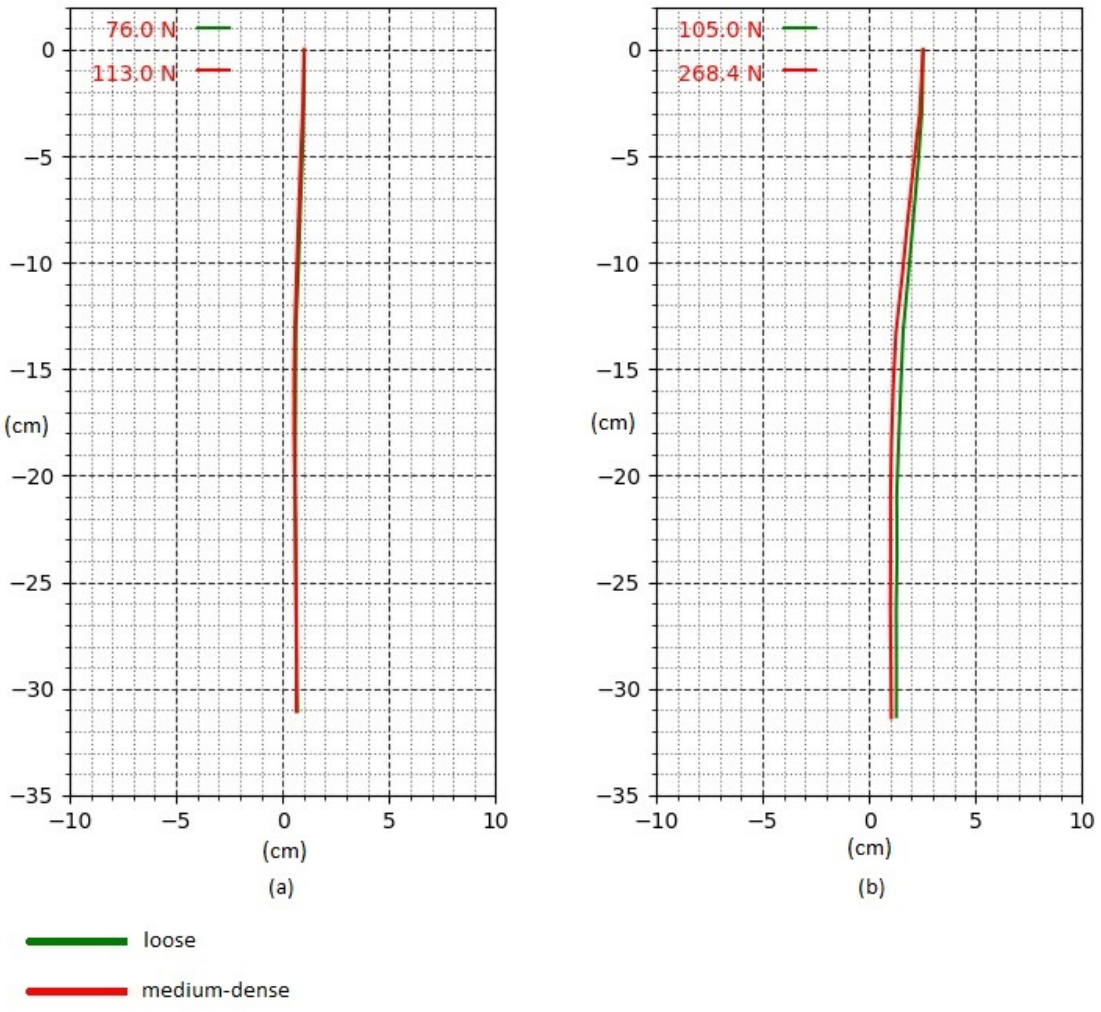

Figure 5.1. 750N Pile in loose and medium-dense sand with 10 (a) and 25 (b) mm displacements.

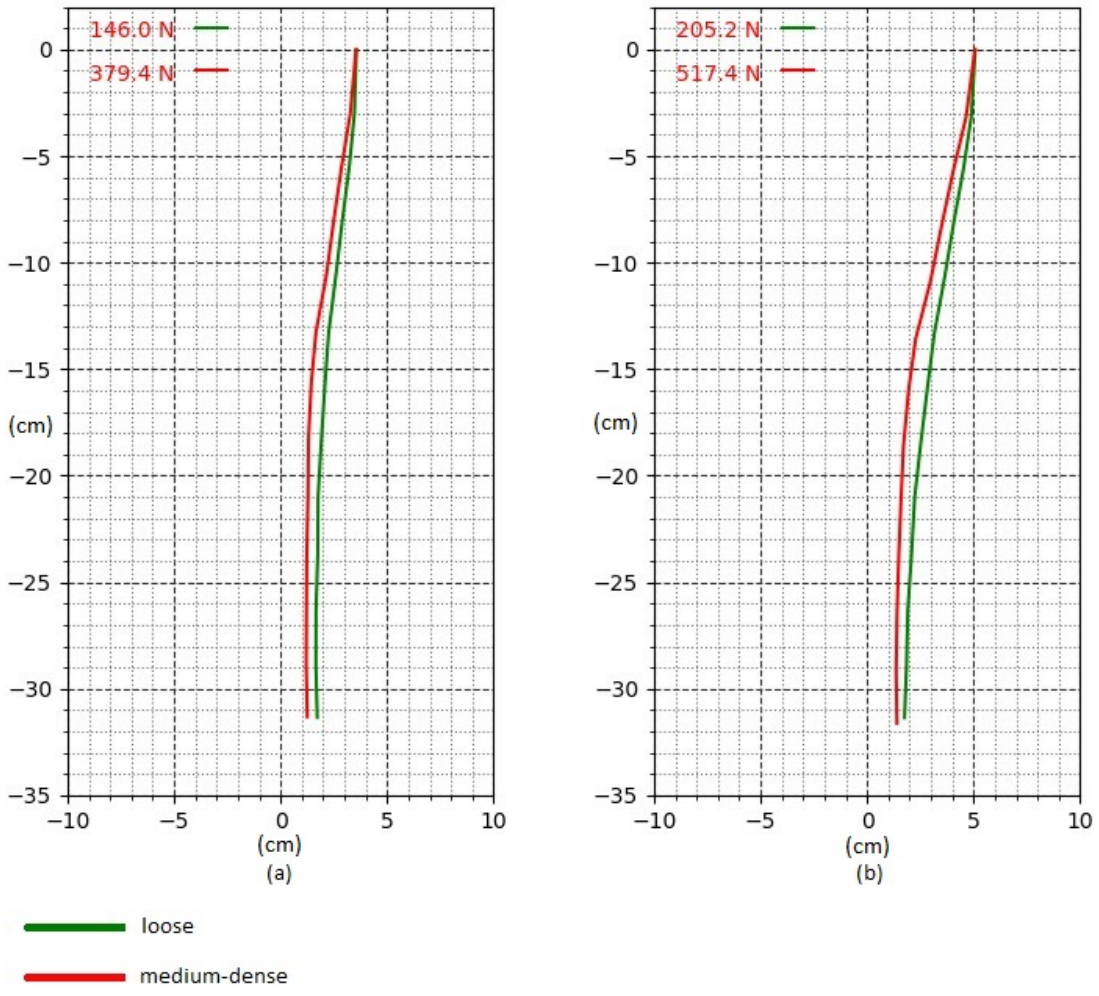

Figure 5.2. 750N Pile in loose and medium-dense sand with 35 (a) and 50 (b) mm displacements.

Table 5.1. Pile head resistance values for 10, 25, 35, and 50 mm pile head displacement in loose and medium-dense sand.

Displacement (mm)	**Loose (N)**	**Medium-dense (N)**	**Ratio**
10	76.0	113.0	1.49
25	105.0	268.4	2.56
35	146.0	379.4	2.60
50	205.2	517.4	2.52

A decrease in the capacity ratio is observed for 2250 N pile with increasing lateral displacement. Even 750 N segmental pile performs well when the soil is medium dense. Although the pile is classified as a short pile its behavior is similar to that of flexible pile except for 2250 N pile installed in loose sand where the pile rotates like a rigid pile. Head load values and ratios are given in Table 5.2 .

Although the E_p/E_s ratio of in medium-dense sand to that of loose sand is approximately 0.50 for both 750 N and 2250 N pile, the pile head load ratios in medium-dense sand to that of loose sand increasing displacement. For 750 N it increases by 70 % while a decrease of 65 % is observed for 2250 N pile. The effect of the relative density of sand around 750 N pile is more effective than that of 2250 N pile.

Table 5.2. Pile head resistance values for 10, 25, 35, and 50 mm pile head displacement in loose and medium-dense sand.

Displacement (mm)	**Loose (N)**	**Medium-dense (N)**	**Ratio**
10	114.4	314.9	2.75
25	195.8	318.9	1.63
35	265.1	445.4	1.68
50	378.1	637.1	1.69

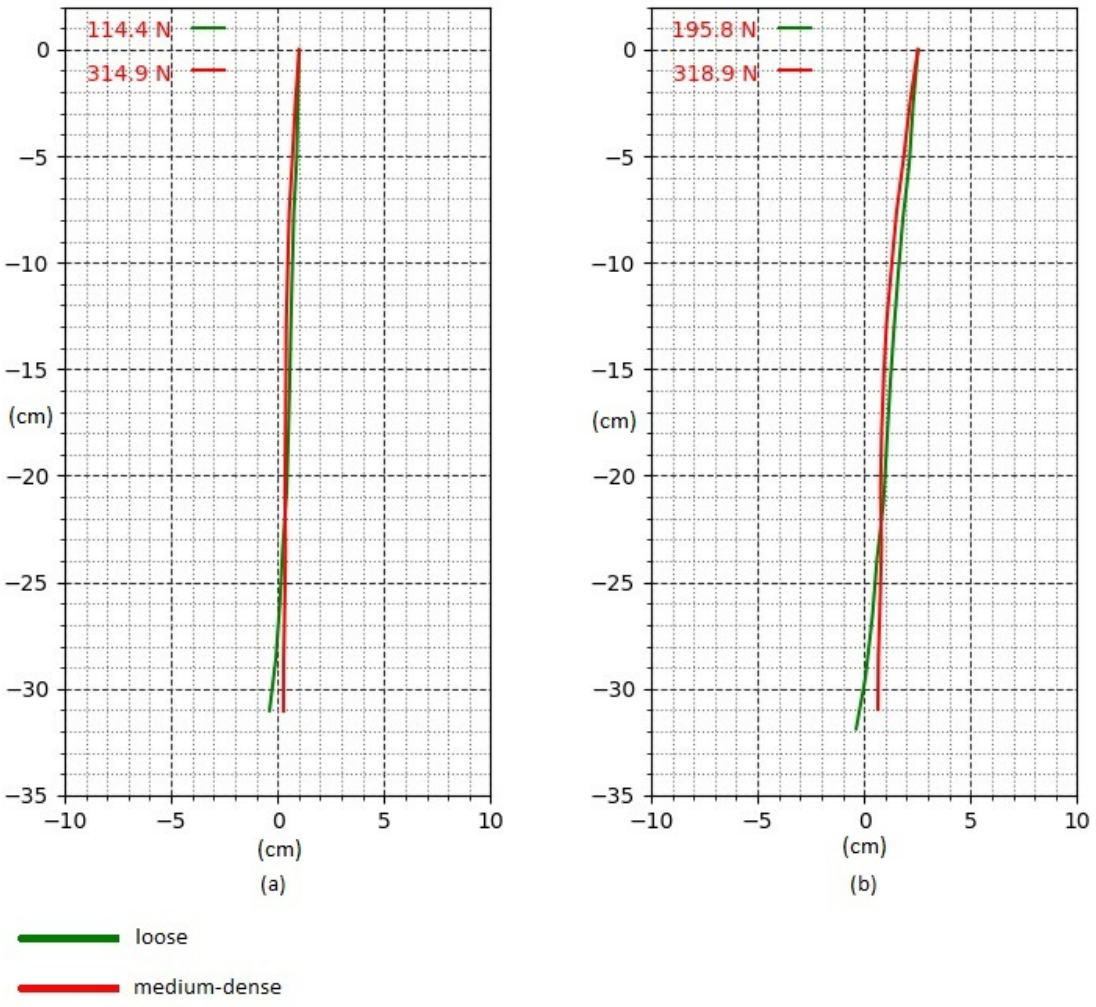

Figure 5.3. 2250N Pile in loose and medium-dense sand with 10 (a) and 25 (b) mm displacements.

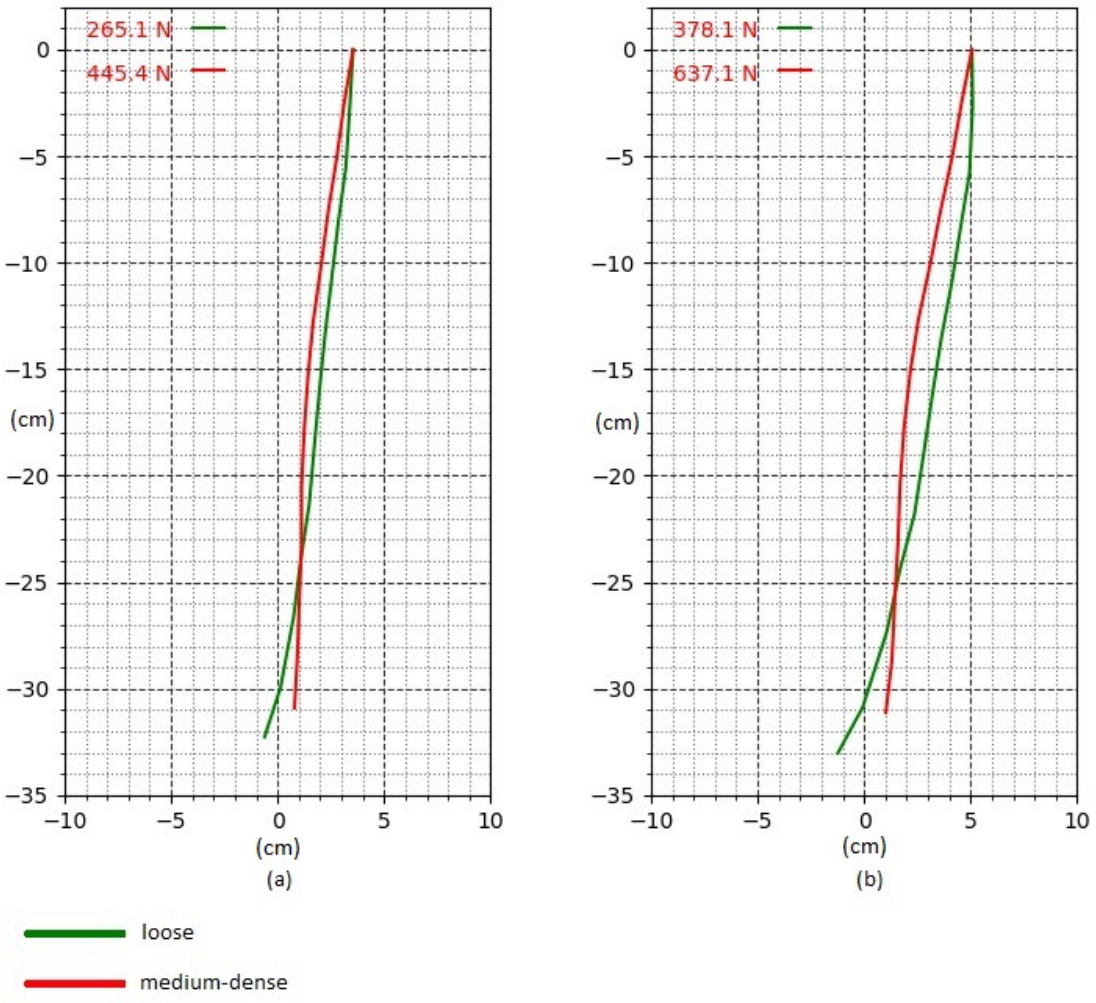

Figure 5.4. 2250N Pile in loose and medium-dense sand with 35 (a) and 50 (b) mm displacements.

5.2. Effect of Flexural Rigidity

The lateral displacement values for 750N and 2250N piles are presented in Figure 5.5 to Figure 5.8. The pile lateral capacity ratio for 2250 N to that of 750 N varies between 1.51 and 1.84 for 10 mm and 50 mm displacement in loose soil. In dense soil, the same ratio decreases to 1.23 at 50 mm displacement. When the soil modulus increases the 750 N pile reaches 85 percent of the capacity of 2250 N pile. The plastic hinge in the medium-dense sand was observed at the similar depth of both piles.

Figure 5.8 presents lateral pile displacements through pile height and lateral load at pile head when the pile head displaced 35 mm and 50 mm respectively.

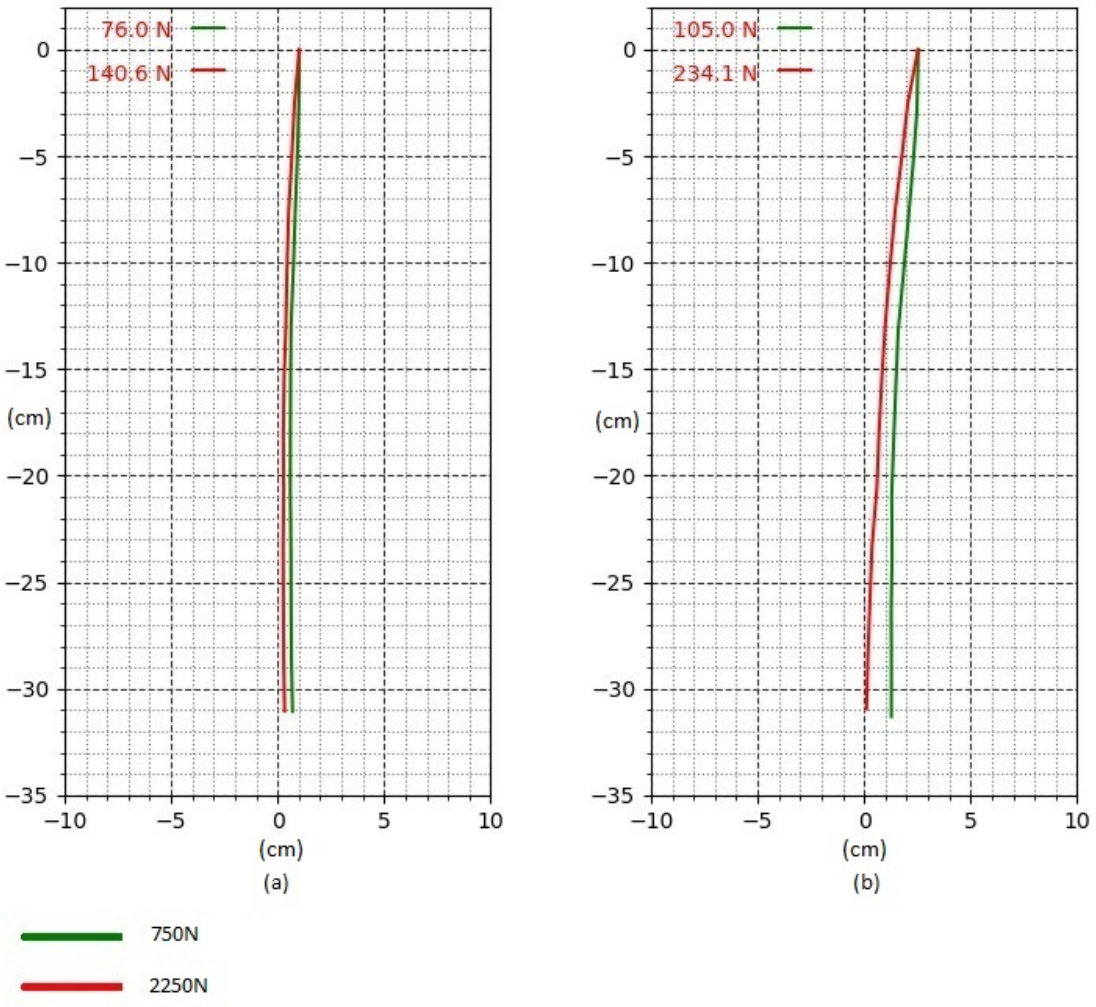

Figure 5.5. 750N and 2250N piles in loose sand with 10 (a) and 25 (b) mm displacements.

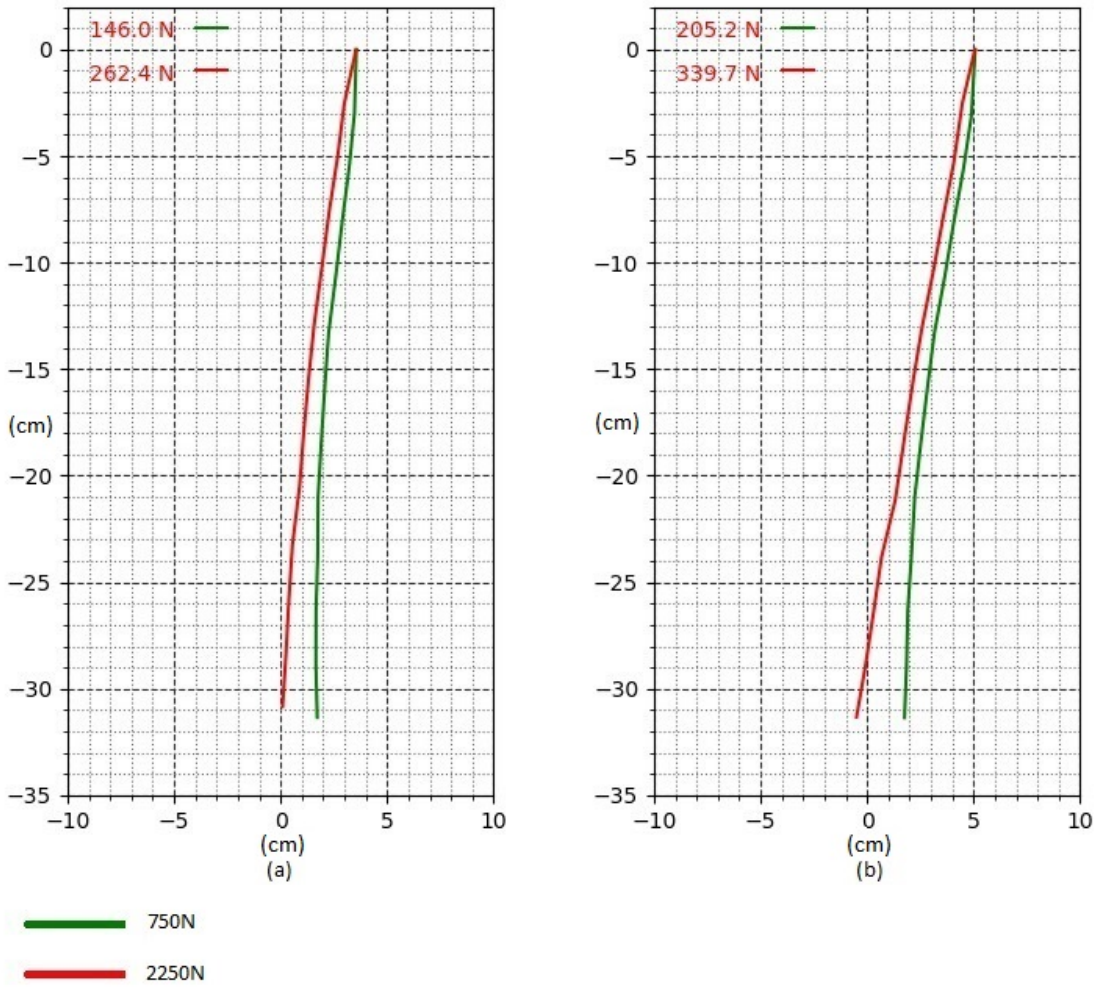

Figure 5.6. 750N and 2250N piles in loose sand with 35 (a) and 50 (b) mm displacements.

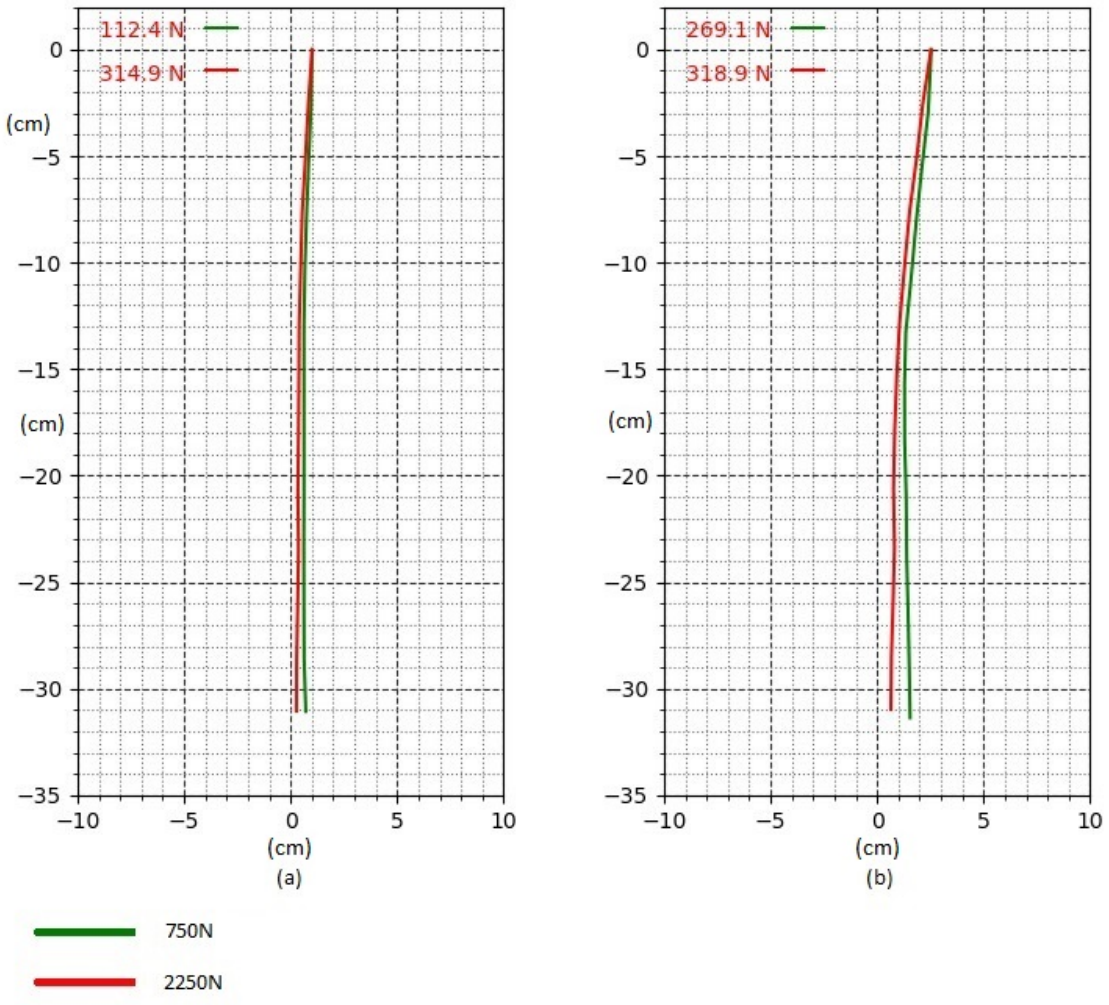

Figure 5.7. 750N and 2250N piles in medium-dense sand with 10 (a) and 25 (b) mm displacements.

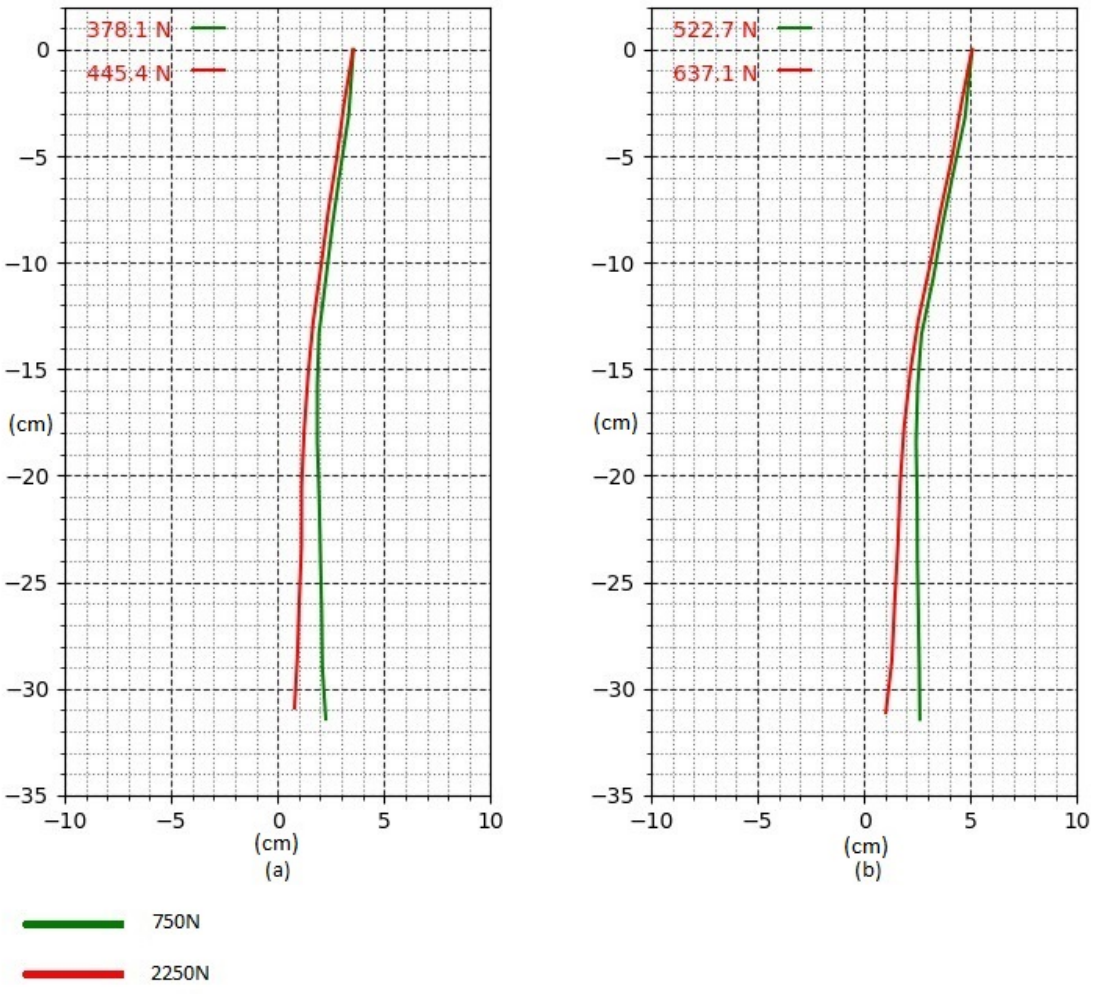

Figure 5.8. 750N and 2250N piles in medium-dense sand with 35 (a) and 50 (b) mm displacements.

5.3. Pile Base Shifting

In the results of 750 N pile in loose and medium-dense sand, it is observed that the pile base shifted with pile head displacement. The pile base displacement values are shown in Figure 5.9. Displacement values are discussed in the next section.

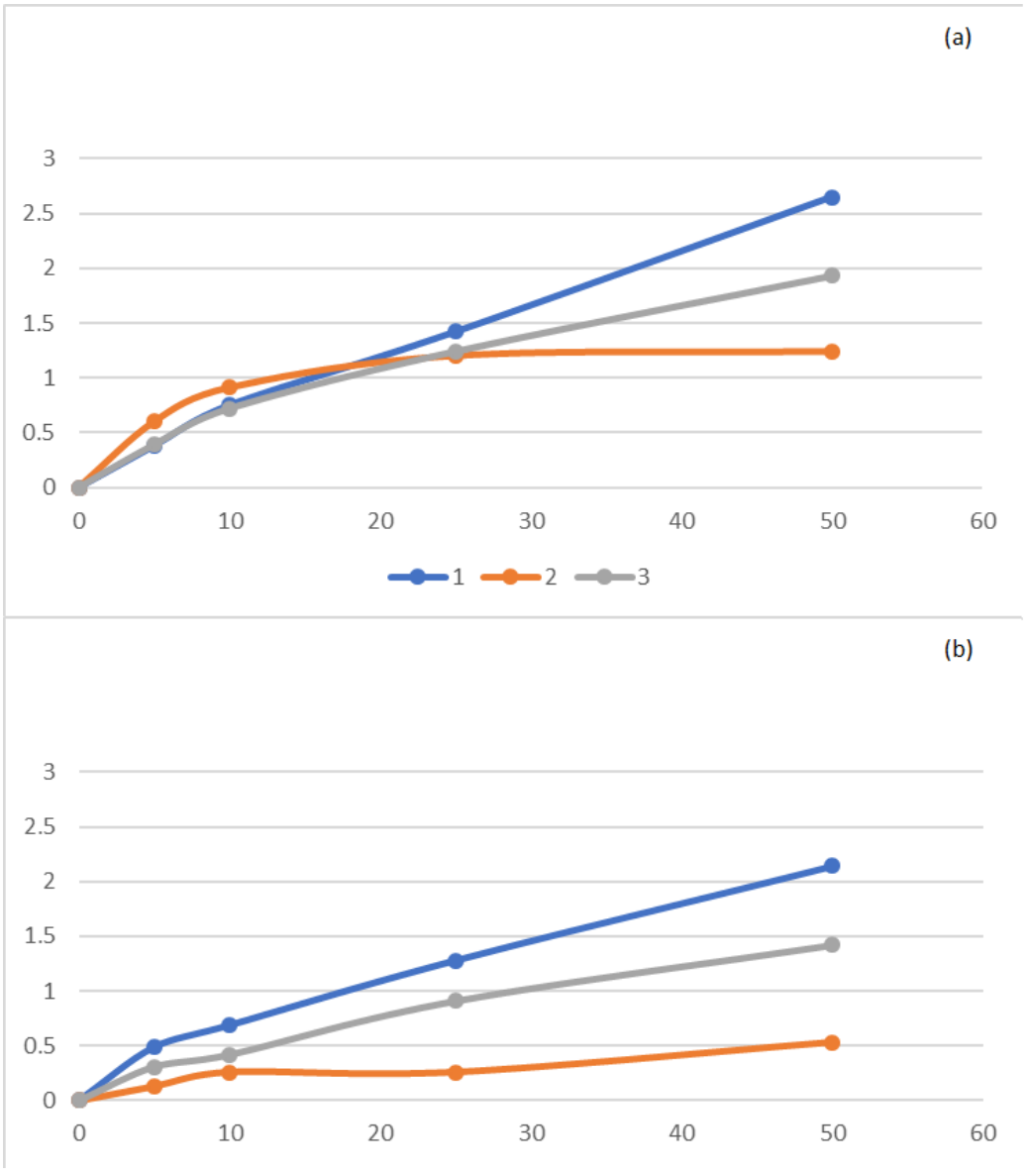

Figure 5.9. The base displacement (mm) of the pile with 750 N post-tension in loose (a) and medium-dense (b).

5.4. Earth Pressure on the Pile

For each experiment, Mei's earth pressures at the loaded front of the pile are calculated and compared with the measured pile head load. To calculate lateral earth pressure, Rankine's earth pressure coefficients were obtained from Kerisel and Absi's tables [15]. For each block, K_p was obtained from the proper table according to the friction angle of soil, angle of the plane OB with the vertical plane, angle of the plane OB with the vertical plane, the slope of the free surface OA in respect to the horizontal line, inclination of the overburden pressure, and inclination of the active or passive earth pressure on the plane OB as planes are shown in Figure 5.10.

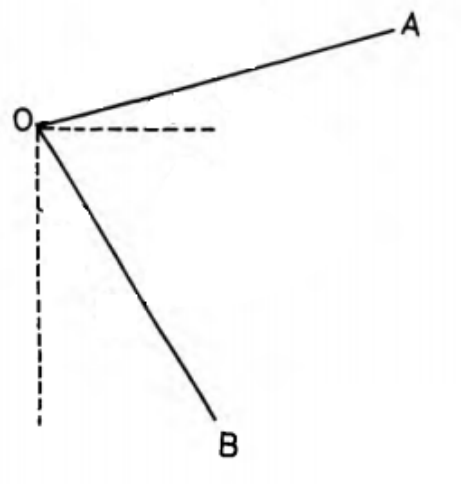

Figure 5.10. Planes of slope [15].

For the pile post-tensioned 750 N in loose and medium-dense sand, earth pressures and pile head loads are given in Figure 5.11 and Table 5.3. Calculations for the pile post-tensioned 750 N in loose and medium-dense sand, shifting under the bending point was neglected.

Verification is needed by measuring soil reaction in front of the pile. A rough approach has been implemented with the results obtained in this section. These initial results are not conclusive and should be treated with care.

Table 5.3. Earth pressure and measured head load of 750 N pile in loose and medium-dense sand.

Displ. (mm)	**Earth pressure (loose)**	**Head load (loose)**	**Earth pressure (medium-dense)**	**Head load (medium-dense)**
5	75.3	66.6	84.8	100.2
10	122.7	111.7	144.5	156.8
15	160.9	137.2	209.6	197.1
20	198.5	155.4	282.0	275.8
25	242.8	192.4	345.4	316.9
30	263.3	219.3	418.5	407.0
35	295.4	265.7	493.0	472.0
40	331.5	299.4	562.8	571.0
45	358.5	339.0	637.9	656.0
50	362.3	370.0	702.1	697.0

For the pile post-tensioned 2250 N in loose and medium-dense sand, earth pressures and pile head loads are given in Figure 5.12 and Table 5.4.

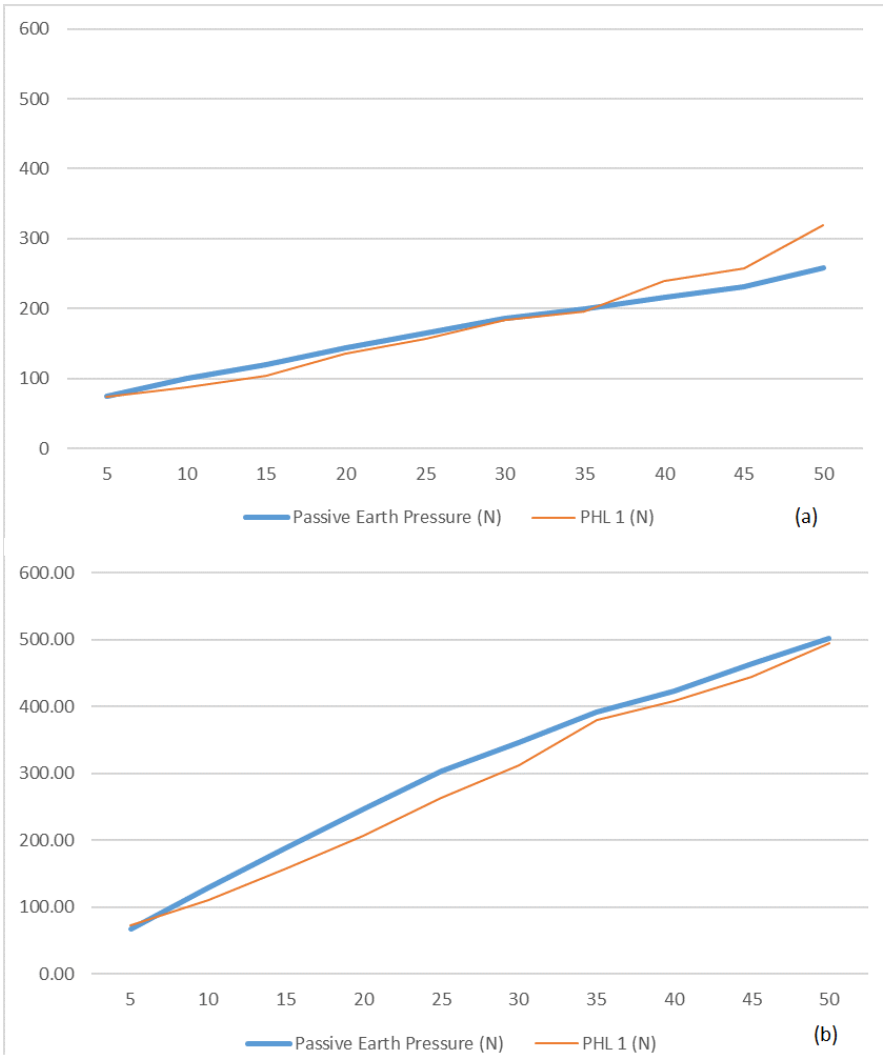

Figure 5.11. Earth pressure (N) and measured pile head load (PHL) (N) of 750 N pile in loose (a) and medium-dense (b) sand.

Table 5.4. Earth pressure and measured head load of 2250 N pile in loose and medium-dense sand.

Displ. (mm)	**Earth pressure (loose)**	**Head load (loose)**	**Earth pressure (medium-dense)**	**Head load (medium-dense)**
5	73.9	73.3	54.5	47.0
10	100.8	87.5	76.0	83.0
15	120.4	104.3	91.5	92.8
20	143.3	135.2	89.5	95.9
25	165.0	156.1	105.0	104.2
30	186.7	183.7	142.6	142.2
35	199.6	195.8	146.0	154.8
40	216.6	240.0	166.8	173.0
45	231.7	257.0	176.9	185.4
50	259.0	320.0	205.2	214.8

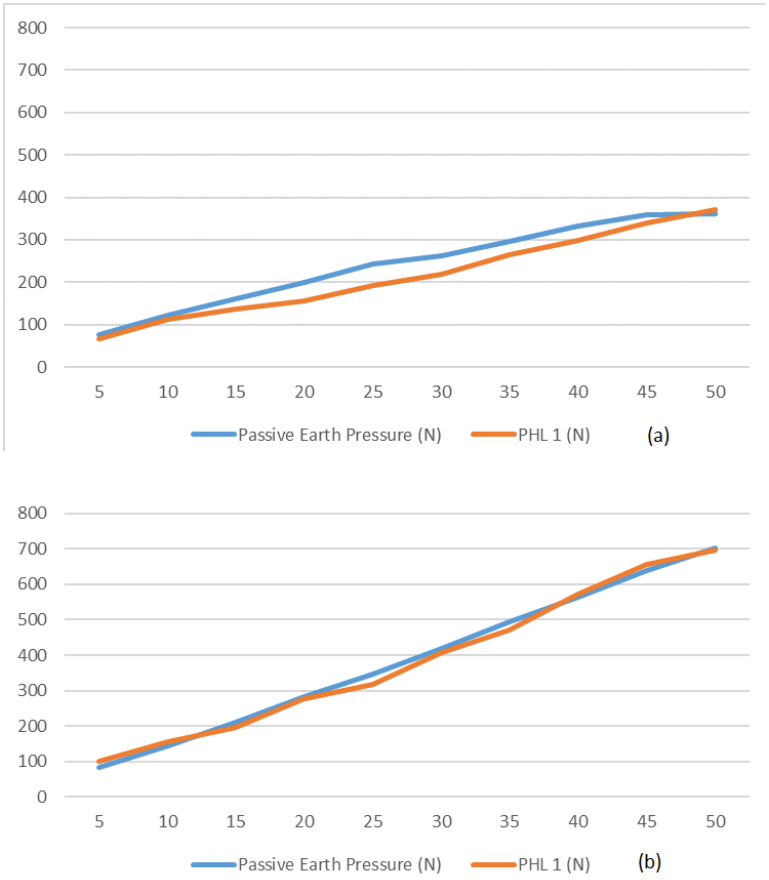

Figure 5.12. Earth pressure (N) and measured pile head load (PHL) (N) of 2250 N pile in loose (a) and medium-dense (b) sand.

5.5. Comparison with Literature

Experiments of Yahia et al. [11] and this study are similar in terms of type, post-tension, and materials of the pile. Major differences are base fixing of the pile, soil, and the loading mechanism. As given in Figure 2.13, the segmental pile with 2250 N post-tension experiment results have similarities with the results of this study. Increasing soil stiffness with springs caused an increase in the flexible behavior of the pile. Since the base of the pile was fixed in experiments of Yahia [11], bending behavior above the bending point is quite different. The pile displacement with depth of this study in medium-dense soil and on Yahia's spring model tests are given in Figure 5.13 for the pile with 2250 N post-tension.

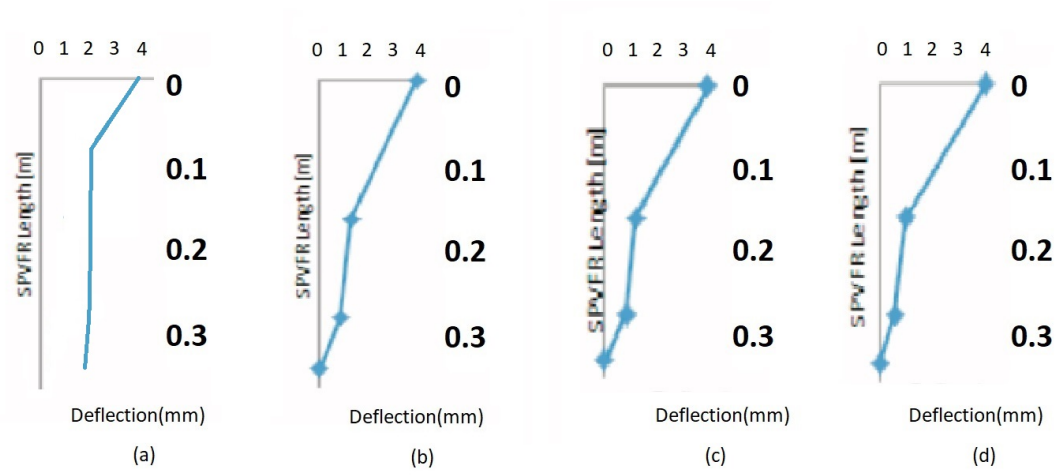

Figure 5.13. Comparison of the pile displacement with depth of this study (a) in medium-dense sand and Yahia with 1K (b), 2K(c) and 3K(d) [11].

Experiments conducted at the same conditions (dimensions, materials, and post-tensions of piles, soil, and test box) with Sengez et al. except the loading mechanism and measurement system. While the constant strain was applied to the pile head and head-load was measured at this study, Sengez et al. constant load (300 N) applied to the pile head cyclically. Sengez et al. applied 300 N head load statically initially and this part of the experiments is similar to experiments of this study. A comparison of displacement of pile head corresponds to 300 N head-load is shown in Table 5.5. Displacements of the measured and results of Sengez are significantly different. The loading mechanism and displacement measurement may have been the problem.

Table 5.5. Comparison of displacement of pile head correspond 300 N head-load.

Pile (N)	**Relative Density**	**Displacement Sengez [12](mm)**	**Displacement Measured (mm)**	**K_{rc}**
750	loose	2.2	41.2	$2.1x10^{-3}$
750	medium-dense	2.14	27.97	$1.1x10^{-3}$
2250	loose	2.2	35.57	$5.7x10^{-3}$
2250	medium-dense	2.16	19.42	$3.0x10^{-3}$

The effect of relative density on lateral movement is also considered in the study. According to the results of Kim and Youn [10], the Increase of relative density from 27 % to 50% caused an increase of load from 38.4 to 52.8 N for 8 mm head displacement. According to this study, the increase of relative density from loose to medium-dense caused an increase of the pile head load from 80 to 112 N for the pile with 750 N post-tension and from 130 to 200 N for the pile with 2250 N post-tension.

6. CONCLUSIONS

The conclusions given below are limited to the tests conducted. Some verification tests were not completed due to pandemic restrictions. Segmental model piles are composed of alternating concrete blocks and rubber sheets connected by a steel wire which can be tensioned to a desired force. Segmental piles with 750N and 2250N post-tension force were placed into loose and medium dense sand and 50 mm lateral displacement was applied. The pile head load was measured. The segmental piles underwent displacements as large as their width with no failure. The large displacement capability of segmental piles without failure will have several implementations to resist lateral loads. The lateral capacity of piles reached up to 700 N for 2250N pile in medium dense sand demonstrating the capability of these types of piles under large displacements.

The lateral displacement along the pile was obtained by large number of low-cost sensors revealing the shape of the deformed pile installed in sand. Magnetometers placed on each concrete block were calibrated to obtain the inclination of each block and an algorithm was developed to calculate lateral displacements along the pile from inclinations. The standard deviation values of inclination were 0.36, 0.60, and 1.71 degrees for 7.5, 15, and 22.5 degrees of inclination values respectively. Using large number of low-cost sensors proved to be an optimal solution for the determination of the deformed pile shape and has good potential for geotechnical implementation.

Although the L/D ratio of the piles was relatively small, The 750N segmental pile demonstrated a flexible pile behavior for loose and dense sand conditions. The 2250 N segmental pile behaved similarly to that of a rigid pile for loose sand condition. For the medium dense sand, the behavior changed to that of a flexible pile. The horizontal capacity of 750 N pile reached to 500N for medium dense sand at 50 mm displacement coming close to 700N load measured for 2250N segmental pile under similar conditions.

Monolithic concrete piles with the same dimensions should be tested under the same testing conditions to be able to validate the obtained results. The use of more advanced economic sensors with self-calibration capability, with gyroscope and accelerometer, is recommended. Improvements for the fixed pile head connection to the loading mechanism is recommended. The free connection also should be studied. The pile tip movement should be directly measured.

REFERENCES

1. Reese, L. C., S. Wang, W. Isenhower and J. Arrellaga, "Computer program Lpile plus version 5.0 technical manual", *Ensoft: Austin, TX, USA*, 2004.

2. Van Impe, W. F. and L. C. Reese, *Single piles and pile groups under lateral loading*, CRC press, 2010.

3. Viggiani, C., A. Mandolini and G. Russo, *Piles and pile foundations*, CRC Press, 2014.

4. Broms, B. B., "Lateral resistance of piles in cohesive soils", *Journal of the Soil Mechanics and Foundations Division*, Vol. 90, No. 2, pp. 27–64, 1964.

5. Rao, S. N., V. Ramakrishna and M. B. Rao, "Influence of rigidity on laterally loaded pile groups in marine clay", *Journal of Geotechnical and Geoenvironmental Engineering*, Vol. 124, No. 6, pp. 542–549, 1998.

6. Mayne, P. W., F. H. Kulhawy and C. H. Trautmann, "Laboratory modeling of laterally-loaded drilled shafts in clay", *Journal of geotechnical engineering*, Vol. 121, No. 12, pp. 827–835, 1995.

7. Khari, M., K. A. Kassim and A. Adnan, "An experimental study on pile spacing effects under lateral loading in sand", *The Scientific World Journal*, Vol. 2013, 2013.

8. Patra, N. R. and P. J. Pise, "Ultimate lateral resistance of pile groups in sand", *Journal of Geotechnical and Geoenvironmental Engineering*, Vol. 127, No. 6, pp. 481–487, 2001.

9. Prasad, Y. V. and T. Chari, "Lateral capacity of model rigid piles in cohesionless soils", *Soils and Foundations*, Vol. 39, No. 2, pp. 21–29, 1999.

10. Kim, B. T. and G. L. Yoon, "Laboratory modeling of laterally loaded pile groups in sand", *KSCE journal of Civil Engineering*, Vol. 15, No. 1, pp. 65–75, 2011.

11. Yahia, Y., *An Experimental Study on the Behavior of Segmental Pile with Variable Flexural Rigidity*, Ph.D. Thesis, Boğaziçi University, 2014.

12. Sengez, M., *Lateral Capacity Of Segmental Model Piles Under Cyclic Loading*, Master's Thesis, Boğaziçi University, Istanbul,Turkey, 2019.

13. Dipova, N., "Açık Kaynaklı Geliştirme Platformlarının Geoteknik Laboratuvarı Çözümlerinde Kullanımı", *Mehmet Akif Ersoy Üniversitesi Fen Bilimleri Enstitüsü Dergisi*, Vol. 8, No. 2, pp. 153–160, 2017.

14. Camps, F., S. Harasse and A. Monin, "Numerical calibration for 3-axis accelerometers and magnetometers", *IEEE International Conference on Electro/Information Technology*, pp. 217–221, 2009.

15. Absi, E., *Active and Passive Earth Pressure Tables*, Routledge, 2017.

16. Mei, G., Q. Chen and L. Song, "Model for predicting displacement-dependent lateral earth pressure", *Canadian geotechnical journal*, Vol. 46, No. 8, pp. 969–975, 2009.

17. Poulos, H. G. and E. H. Davis, *Pile Foundation Analysis and Design*, Monograph, Wiley, 1980.

18. Qin, H. and W. D. Guo, "Nonlinear response of laterally loaded rigid piles in sand", *Geomechanics and Engineering*, Vol. 7, pp. 679–703, 2014.

19. Fan, C.-C. and J. H. Long, "Assessment of existing methods for predicting soil response of laterally loaded piles in sand", *Computers and Geotechnics*, Vol. 32, No. 4, pp. 274–289, 2005.

20. Baykal, G., *Ankraj Kablosu Germeli Eklemli Kazık Sistemi Geliştirilmesi*, Tech.

Rep., Boğaziçi Üniversitesi Bilimsel Araştırma Projeleri, 2011.

21. Brinch Hansen, J., "The Ultimate Resistance of Riged Piles Against Transversal Forces", *Danish Geotechnical Institute(Geoteknik Institut)*, Vol. 12, 1961.

22. Broms, B. B., "Lateral resistance of piles in cohesionless soils", *Journal of the Soil Mechanics and Foundations Division*, Vol. 90, No. 3, pp. 123–158, 1964.

23. Broms, B. B., "Design of laterally loaded piles", *Journal of Soil Mechanics & Foundations Div*, Vol. 92, pp. 75–76, 1966.

24. Winkler, E., *Die Lehre von der Elasticitaet und Festigkeit: mit besonderer Rücksicht auf ihre Anwendung in der Technik für polytechnische Schulen, Bauakademien, Ingenieue, Maschinenbauer, Architecten, etc*, Vol. 1, Dominicus, 1867.

25. Hetenyi, M., *Beams on elastic foundation: theory with applications in the fields of civil and mechanical engineering*, Ann Arbor : University of Michigan Press, 1946.

26. Granholm, H., *On the Elastic Stability of Piles Surrounded by a Supporting Medium*, Svenska Bokhandelscentralen A.-B, 1929.

27. Terzaghi, K., "Evalution of conefficients of subgrade reaction", *Geotechnique*, Vol. 5, No. 4, pp. 297–326, 1955.

28. Matlock, H. and L. C. Reese, "Generalized solutions for laterally loaded piles", *Transactions of the American Society of Civil Engineers*, Vol. 127, No. 1, pp. 1220–1247, 1962.

29. Palmer, L. and J. Thompson, "The earth pressure and deflection along the embedded lengths of piles subjected to lateral thrusts", *Proc, 2nd Int. Conf. Soil Mech. and Found. Eng., GEBR Kesmat, Haarlem, The Netherlands*, Vol. 5, pp. 156–161, 1948.

30. Davisson, M. and S. Prakash, "A review of soil-pole behavior", N. R. Council (Editor), *Stresses in Soils and Layered Systems*, pp. 25–48, Highway Research Board, Washington, D.C, 1963.

31. Dash, S., M. Rouholamin, D. Lombardi and S. Bhattacharya, "A practical method for construction of py curves for liquefiable soils", *Soil Dynamics and Earthquake Engineering*, Vol. 97, pp. 478–481, 2017.

32. McClelland, B. *et al.*, "Soil modulus for laterally loaded piles", *Journal of the Soil Mechanics and Foundations division*, Vol. 82, No. 4, pp. 1–22, 1956.

33. Matlock, H., "Correlations for design of laterally loaded piles in soft clay", *Proceedings of 2nd Offshore Technology Conference*, pp. 577–594, Dallas, Tex, 1970.

34. Reese, L. C., W. R. Cox, F. D. Koop *et al.*, "Field testing and analysis of laterally loaded piles om stiff clay", *Offshore Technology Conference*, Offshore Technology Conference, 1975.

35. Reese, L. C. and R. C. Welch, "Lateral loading of deep foundations in stiff clay", *Journal of Geotechnical and Geoenvironmental Engineering*, Vol. 101, pp. 633–649, 1975.

36. Reese, L. C., W. R. Cox and F. D. Koop, "Analysis of laterally loaded piles in sand", *Offshore Technology in Civil Engineering Hall of Fame Papers from the Early Years*, pp. 95–105, 1974.

37. Lee, P., L. Gilbert *et al.*, "Behavior of laterally loaded pile in very soft clay", *11th Offshore Technology Conference*, pp. 387–395, OTC, Houston, TEX, 1979.

38. Georgiadis, M., "Development of py curves for layered soils", *Proceedings of the Conference on Geotechnical Practice in Offshore Engineering*, pp. 536–545, ASCE, Reston, VA, 1983.

39. Chong, W., A. Haque, P. Ranjith and A. Shahinuzzaman, "Effect of joints on p–y behaviour of laterally loaded piles socketed into mudstone", *International Journal of Rock Mechanics and Mining Sciences*, Vol. 48, No. 3, pp. 372–379, 2011.

40. Zhang, L., M. C. McVay and P. W. Lai, "Centrifuge modelling of laterally loaded single battered piles in sands", *Canadian Geotechnical Journal*, Vol. 36, No. 6, pp. 1074–1084, 1999.

41. Zhang, L., H. Ernst and H. H. Einstein, "Nonlinear analysis of laterally loadedrock-socketed shafts", *Journal of Geotechnical and Geoenvironmental Engineering*, Vol. 126, No. 11, pp. 955–968, 2000.

42. Mokwa, R. L., J. M. Duncan and M. J. Helmers, "Development of py curves for partly saturated silts and clays", *Proceedings of Sessions of Geo-Denver 2000*, pp. 224–239, ASCE, Denver, CO, 2000.

43. Evans Jr, L. and G. Duncan, *Simplified analysis of laterally loaded piles*, Tech. Rep., UCB/GT/82-04, University of California, Berkeley, CA, 1982.

44. Rollins, K. M., T. M. Gerber, J. D. Lane and S. A. Ashford, "Lateral resistance of a full-scale pile group in liquefied sand", *Journal of Geotechnical and Geoenvironmental Engineering*, Vol. 131, No. 1, pp. 115–125, 2005.

45. Chang, B. and T. Hutchinson, "Experimental evaluation of p-y curves considering development of liquefaction", *Journal of Geotechnical and Geoenvironmental Engineering*, Vol. 139, No. 4, pp. 577–586, 2012.

46. Zhu, B., Y. Sun, R. Chen, W. Guo and Y. Yang, "Experimental and analytical models of laterally loaded rigid monopiles with hardening p–y curves", *Journal of Waterway, Port, Coastal, and Ocean Engineering*, Vol. 141, No. 6, p. 04015007, 2015.

47. Lin, C., J. Han, C. Bennett and R. L. Parsons, "Analysis of laterally loaded piles

in soft clay considering scour-hole dimensions", *Ocean Engineering*, Vol. 111, pp. 461–470, 2016.

48. Suleiman, M. T., L. Ni, J. D. Helm and A. Raich, "Soil-pile interaction for a small diameter pile embedded in granular soil subjected to passive loading", *Journal of Geotechnical and Geoenvironmental Engineering*, Vol. 140, No. 5, p. 04014002, 2014.

49. Ito, T. and T. Matsui, "Methods to estimate lateral force acting on stabilizing piles", *Soils and Foundations*, Vol. 15, No. 4, pp. 43–59, 1975.

50. Mindlin, R. D., "Force at a point in the interior of a semi-infinite solid", *Physics*, Vol. 7, No. 5, pp. 195–202, 1936.

51. Spillers, W. R. and R. D. Stoll, "Lateral response of piles", *Journal of the Soil Mechanics and Foundations Division*, Vol. 90, No. 6, pp. 1–10, 1964.

52. Poulos, H. G., "Behavior of laterally loaded piles I. single piles", *Journal of Soil Mechanics & Foundations Div*, Vol. 97, pp. 711–731, 1971.

53. Poulos, H. G., "Behavior of laterally loaded piles II. Pile groups", *Journal of Soil Mechanics & Foundations Div*, Vol. 97, pp. 711–731, 1971.

54. Poulos, H. G., "Behavior of laterally loaded piles: III—socketed piles", *Journal of the Soil Mechanics and Foundations Division*, Vol. 98, No. 4, pp. 341–360, 1972.

55. Poulos, H. G., "Analysis of piles in soil undergoing lateral movement", *Journal of Soil Mechanics & Foundations Div*, Vol. 99, pp. 391–406, 1973.

56. Banerjee, P. and T. Davies, "The behaviour of axially and laterally loaded single piles embedded in nonhomogeneous soils", *Geotechnique*, Vol. 28, No. 3, pp. 309–326, 1978.

57. Davies, T. and M. Budhu, "Non-linear analysis of laterally loaded piles in heavily

overconsolidated clays", *Geotechnique*, Vol. 36, No. 4, pp. 527–538, 1986.

58. Budhu, M. and T. G. Davies, "Nonlinear analysis of laterality loaded piles in cohesionless soils", *Canadian Geotechnical Journal*, Vol. 24, No. 2, pp. 289–296, 1987.

59. Budhu, M. and T. G. Davies, "Analysis of laterally loaded piles in soft clays", *Journal of Geotechnical Engineering*, Vol. 114, No. 1, pp. 21–39, 1988.

60. Randolph, M. F., "The response of flexible piles to lateral loading", *Geotechnique*, Vol. 31, No. 2, pp. 247–259, 1981.

61. Sun, K., "Laterally loaded piles in elastic media", *Journal of Geotechnical Engineering*, Vol. 120, No. 8, pp. 1324–1344, 1994.

62. Vallabhan, C. G. and Y. Das, "Parametric study of beams on elastic foundations", *Journal of Engineering Mechanics*, Vol. 114, No. 12, pp. 2072–2082, 1988.

63. Guo, W. D. and F. Lee, "Load transfer approach for laterally loaded piles", *International Journal for Numerical and Analytical Methods in Geomechanics*, Vol. 25, No. 11, pp. 1101–1129, 2001.

64. Basu, D. and R. Salgado, "Elastic analysis of laterally loaded pile in multi-layered soil", *Geomechanics and Geoengineering: An International Journal*, Vol. 2, No. 3, pp. 183–196, 2007.

65. Prakash, S., *Behavior of Pile Groups Subjected to Lateral Loads*, University of Illinois, 1962.

66. Meyerhof, G. G., "Scale effects of ultimate pile capacity", *Journal of Geotechnical Engineering*, Vol. 109, No. 6, pp. 797–806, 1983.

67. Lin, H., L. Ni, M. T. Suleiman and A. Raich, "Interaction between laterally loaded pile and surrounding soil", *Journal of Geotechnical and Geoenvironmental Engi-*

neering, Vol. 141, No. 4, p. 04014119, 2014.

68. Chawhan, B., S. Quadri and P. Rakaraddi, "Behavior of Lateral Resistance of Flexible Piles in Layered Soils", *Journal of Mechanical and Civil Engineering*, Vol. 2, pp. 7–11, IGC, 2012.

69. Mohamedzein, Y. E., F. Nour Eldaim and A. Abdelwahab, "Laboratory model tests on laterally loaded piles in plastic clay", *International Journal of Geotechnical Engineering*, Vol. 7, No. 3, pp. 241–250, 2013.

70. Baykal, G., "Large Displacement, Constant Contact Area Geosynthetic-Soil Interface Direct Shear Test Device", *Proceedings of the 19th International Conference on Soil Mechanics and Geotechnical Engineering*, pp. 1337–1340, ISSMGE, Seoul, 2017.

71. D'Ausilio, A., "Arduino: A low-cost multipurpose lab equipment", *Behavior Research Methods*, Vol. 44, No. 2, pp. 305–313, 2012.

72. Masi, M., F. Ferdos, G. Losito and L. Solari, "Development of an Arduino-based electrical impedance tomography system with application to dam internal erosion detection", *EGU General Assembly Conference Abstracts*, Vol. 18, 2016.

73. Malatinec, T., V. Popelka, M. Huba and P. Hudačko, "Laboratory model helicopter control using a lowcost Arduino hardware", *15th International Carpathian Control Conference (ICCC)*, pp. 326–331, IEEE, 2014.

74. Candelas, F., G. J. García, S. Puente, J. Pomares, C. Jara, J. Pérez, D. Mira and F. Torres, "Experiences on using Arduino for laboratory experiments of Automatic Control and Robotics", *IFAC-PapersOnLine*, Vol. 48, No. 29, pp. 105–110, 2015.

75. Costanzo, A., "An arduino based system provided with GPS/GPRS shield for real time monitoring of traffic flows", *7th International Conference on Application of Information and Communication Technologies*, pp. 1–5, 2013.

76. Sun, Z., S. J. Dyke, F. Pena and A. Wilbee, "Development of Arduino based wireless control system", *Sensors and Smart Structures Technologies for Civil, Mechanical, and Aerospace Systems 2015*, Vol. 9435, p. 94351D, International Society for Optics and Photonics, 2015.

77. Lekshmi, K. A. and D. Arnepalli, "A Methodology to Determine Water Vapour Diffusion Characteristics of Geomaterials", *Geotechnical Characterisation and Geoenvironmental Engineering*, pp. 131–137, Springer, 2019.

78. Raybould, D., D. Price *et al.*, "The use of the proton magnetometer in engineering geological investigations", *1st ISRM Congress*, International Society for Rock Mechanics and Rock Engineering, 1966.

79. Deans, C., L. Marmugi and F. Renzoni, "Active underwater detection with an array of atomic magnetometers", *Applied Optics*, Vol. 57, No. 10, pp. 2346–2351, 2018.

80. Koerner, R., "Use of a proton precession magnetometer to detect buried drums in sandy soil", *Journal of Hazardous Materials*, Vol. 8, pp. 11–23, 1983.

81. *Standard Specification for Mortar for Unit Masonry*, Standard, American Society for Testing and Materials(ASTM), West Conshohocken, PA.

82. *Standard Practice for Classification of Soils for Engineering Purposes*, Standard, American Society for Testing and Materials(ASTM), West Conshohocken, PA.

83. Predko, M., *Programming and Customizing PICmicro Microcontrollers*, McGraw-Hill Professional, 2000.

84. Crassidis, J. L., K.-L. Lai and R. R. Harman, "Real-time attitude-independent three-axis magnetometer calibration", *Journal of Guidance, Control, and Dynamics*, Vol. 28, No. 1, pp. 115–120, 2005.

APPENDIX A: ADDITIONAL RESULTS

A.1. Inclinations of the Pile Blocks

Inclinations of the pile blocks for experiments are given in Figure A.1, A.2, A.3, and A.4. Inclinations are given by the pile head displacement.

Table A.1. Individual inclinations of the pile blocks of EXP#1.

Block	**5 mm**	**10 mm**	**15 mm**	**20 mm**	**25 mm**	**30 mm**	**35 mm**	**40 mm**	**45 mm**	**50 mm**
1	0.12	0.86	1.95	2.46	3.28	3.68	4.39	4.99	6.11	7.04
2	0.24	0.57	1.92	1.92	2.70	3.27	4.14	4.82	5.81	6.92
3	0.93	1.79	2.56	2.67	3.25	3.85	4.73	5.86	6.75	7.97
4	0.81	1.76	3.22	4.12	5.05	6.14	6.96	7.65	8.97	9.69
5	0.39	1.55	3.02	3.12	4.05	4.90	5.44	6.25	6.85	7.34
6	0.14	2.20	2.99	4.58	7.05	8.44	8.89	10.78	11.89	14.15
7	-0.09	0.88	1.23	2.25	3.45	4.43	4.85	6.01	6.62	7.87
8	-0.32	-0.45	-0.52	-0.08	-0.15	0.41	0.81	1.25	1.35	1.58
9	-0.22	-0.03	0.15	-0.04	0.31	0.13	0.22	0.36	0.51	0.61
10	-0.44	-0.82	0.01	-0.57	0.32	0.11	0.51	0.74	1.20	1.33
11	-0.56	-1.19	0.54	-1.07	0.79	-0.19	0.20	0.24	1.04	1.07
12	0.47	-0.46	1.47	0.91	1.02	1.76	1.35	1.72	1.50	1.52

Table A.2. Individual inclinations of the pile blocks of EXP#4.

Block	**5 mm**	**10 mm**	**15 mm**	**20 mm**	**25 mm**	**30 mm**	**35 mm**	**40 mm**	**45 mm**	**50 mm**
1	0.68	1.55	2.38	3.16	4.22	5.18	6.13	6.00	7.44	8.38
2	0.97	2.01	3.43	4.77	5.91	6.97	8.04	8.73	9.47	11.05
3	0.86	2.65	3.83	5.33	6.70	7.73	8.78	10.05	11.98	13.45
4	0.66	1.90	3.31	4.55	5.61	6.84	8.17	8.43	9.91	11.78
5	0.13	1.19	2.35	4.05	6.05	7.15	7.99	9.21	11.03	13.15
6	-0.32	0.25	1.02	0.77	1.08	1.20	1.75	2.62	3.39	4.31
7	0.16	-0.38	-0.06	-0.15	-0.06	-0.19	-0.17	0.30	0.47	1.06
8	0.65	-1.01	-1.14	-1.07	-1.20	-1.58	-2.08	-2.03	-2.44	-2.19
9	0.04	0.36	-0.39	-0.70	-1.21	-0.91	-0.23	-0.90	-0.88	-0.30
10	-0.03	-1.30	-0.90	-0.79	-1.19	-0.44	-1.30	-1.37	-1.09	-1.15
11	-0.70	-1.59	-0.66	-0.52	-1.19	0.69	-0.51	-0.72	0.26	-0.10
12	-2.09	-1.05	-1.78	-2.24	-0.89	-2.81	-3.69	-4.05	-2.50	-2.27

Table A.3. Individual inclinations of the pile blocks of EXP#7.

Block	**5 mm**	**10 mm**	**15 mm**	**20 mm**	**25 mm**	**30 mm**	**35 mm**	**40 mm**	**45 mm**	**50 mm**
1	0.42	0.74	2.43	3.18	3.15	3.21	2.15	0.98	0.04	-0.54
2	1.17	2.57	4.95	5.74	5.76	6.12	5.58	4.86	4.87	3.99
3	2.35	4.30	6.07	8.05	8.40	9.89	10.27	11.11	11.22	12.07
4	1.54	2.00	3.46	4.95	6.24	7.16	8.47	8.63	9.88	11.09
5	0.69	1.67	2.57	3.59	4.96	6.20	7.34	8.12	9.75	10.86
6	0.39	1.11	1.60	2.83	2.97	5.24	5.67	6.57	7.95	9.06
7	0.62	1.40	1.76	2.62	3.38	5.12	5.21	6.68	7.93	8.91
8	0.86	1.69	1.92	2.41	3.80	4.99	4.75	6.79	7.91	8.76
9	4.71	2.85	5.23	6.20	6.58	7.85	9.61	11.07	12.85	14.75
10	2.06	2.29	3.30	3.51	5.33	6.56	6.94	8.77	10.54	11.73
11	3.25	2.90	4.67	4.62	6.87	8.13	9.13	10.74	13.18	14.70
12	6.22	6.54	7.47	11.02	11.16	16.17	18.99	21.51	25.50	30.13

Table A.4. Individual inclinations of the pile blocks of EXP#10.

Block	**5 mm**	**10 mm**	**15 mm**	**20 mm**	**25 mm**	**30 mm**	**35 mm**	**40 mm**	**45 mm**	**50 mm**
1	1.80	3.04	4.90	6.01	7.06	7.48	7.46	7.91	8.01	8.79
2	2.09	4.28	6.05	7.83	8.83	10.25	10.84	12.25	12.68	13.85
3	2.02	3.93	5.59	7.62	8.88	9.95	11.27	12.50	13.76	14.75
4	0.69	1.92	3.11	4.82	6.39	7.91	9.12	10.50	12.09	13.13
5	0.74	1.66	2.77	4.15	5.95	7.37	8.56	9.79	11.33	12.70
6	0.18	0.77	1.17	2.63	3.05	4.55	5.63	6.94	7.75	8.82
7	0.29	0.84	1.19	2.24	2.19	3.41	4.51	4.81	6.19	6.60
8	0.39	0.91	1.20	1.85	1.33	2.26	3.39	2.69	4.64	4.38
9	-1.20	-1.03	-0.56	-1.19	-0.25	-0.07	0.49	0.28	1.77	2.15
10	0.33	0.46	1.02	0.92	0.99	1.89	3.54	3.05	4.26	4.34
11	0.27	0.02	0.85	0.00	0.65	1.52	3.70	3.41	3.89	4.29
12	-1.07	-2.20	3.53	0.34	-0.80	3.30	2.86	2.60	6.51	6.49

APPENDIX B: EXAMPLE PASSIVE EARTH PRESSURE CALCULATION

An example calculation of lateral earth pressure with the method of Mei et al. [16] for 2250 N pile in loose sand at 15 mm head displacement is shown in Figure B.1. The k_a and k_b values were obtained from the tables of Kerisel and Absi [15].

$$k_p = 13.05$$

$$k_a = 0.178$$

$$k_0 = 0.331$$

$$s_a = -0.00096$$

$$A = \frac{k_p - k_a}{k_p - 2k_0 + k_a} = \frac{12.52 - 0.178}{12.51 - 2(0.331) + 0.178)} = 1.025$$

$$k = \frac{4k_p}{k_0} - 4 = \frac{13.05}{0.331} - 4 = 153.7$$

$$b = \frac{-ln(A)}{s_a} = 26.03$$

$$p_s = \left[\frac{k(\phi)}{1 + e^{-b(s_a, \phi)}} - \frac{k(\phi) - 4}{2}\right]\frac{p_0}{2}$$

$$p_s = \left[\frac{153.69}{1 + e^{26.03}} - \frac{153.69 - 4}{2}\right]\frac{778.8N/m^2}{2} = 13.09kPa$$

$$P = 209.57N$$

$$P_{measured} = 197.1$$

Figure B.1. An example calculation of lateral earth pressure with method of Mei et al. [16].

APPENDIX C: AN EXAMPLE FOR ALGORİTHM

The first experiment of SPVFR with 2250 N post-tension in loose sand is given in this section.

1. Load, V_x,V_y, and V_z values were fetched from database and are shown in Table C.1.

2. For each block, values were calibrated with transformation and bias matrices. Equation for first block (n_0) is given in Equation C.1.

$$\begin{pmatrix} 1390.204 \\ 584.689 \\ 518.608 \end{pmatrix} = \begin{bmatrix} 1.134 & 0.228 & 0.281 \\ -0.425 & 1.535 & 0 \\ -0.259 & -0.012 & 1.738 \end{bmatrix} . \begin{pmatrix} 460 - (-523.323) \\ 679 - (25.840) \\ 974 - (524.905) \end{pmatrix} \tag{C.1}$$

3. With using arctan2 function, slopes were calculated and are shown in Table C.1. Equation for first block (n_0) is given in Equation C.2.

$$arctan2(518.608, 1390.204) = 20.436^{\circ} \tag{C.2}$$

Table C.1. V_x ,V_y ,V_z, offset inclination, and inclination values of blocks.

Block	$\mathbf{V_x}$	$\mathbf{V_y}$	$\mathbf{V_z}$	**Offset inclination**	**Inclination**
1	460	679	974	20.51	-0.084
2	381	666	415	27.306	0.193
3	484	580	103	9.757	1.014
4	375	415	17	6.769	0.776
5	591	550	119	1.779	1.005
6	387	466	-66	6.442	0.673
7	700	-418	-784	-51.362	0.573
8	351	476	90	-5.386	1.932
9	269	289	-21	-17.73	1.932
10	166	204	-19	-16.011	1.602
11	78	71	-141	-22.645	2.632
12	18	2	-99	-57.645	6.550

4. Because location, inclination, height, and width of the first block (n_0) are known, the first block can be located without any other information. Top-right corner x and z coordinates, inclination, height and width of the first block (n_0) are 0.32 cm, 0 cm, 0.084°, 2 cm, and 5 cm respectively. It should not be forgotten that sensor local axes are different from pile axes.

5. Since inclination of second block (n_1) is bigger than previous block (n_0), bottom-left corner of n_0 and top-left corner of n_1 are at same coordinates. From geometrical calculation, that coordinate can be obtained and second block (n_1) can be located. Top-right corner x and z coordinates, inclination, height and width of first block (n_1) are 0.3248 cm, -2.630 cm, 0.193°, 2 cm, and 5 cm respectively.

6. Other blocks were located with the same calculations. Illustration of the pile at 3.2 mm head displacement is shown in Figure C.1 and locations are shown in Table

C.2.

Table C.2. Calculated coordinates and inclinations.

Block	**x coordinate**	**z coordinate**	**Inclination**
1	0.3200	0.0000	-0.084
2	0.3237	-2.6000	0.193
3	0.3155	-5.1300	1.014
4	0.2726	-7.6546	0.776
5	0.2388	-10.2494	1.005
6	0.1926	-12.9790	0.673
7	0.1612	-15.4038	0.573
8	0.1313	-18.0536	1.932
9	0.1057	-20.7085	1.932
10	0.0164	-23.4569	1.602
11	-0.0524	-26.0160	2.632
12	-0.1946	-28.9541	6.550

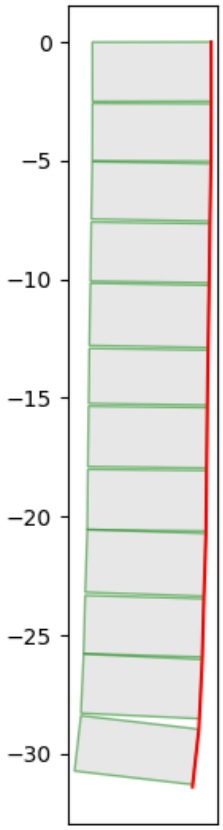

Figure C.1. Illustration of the pile at 3.2 mm head displacement.